

**Analysis of Slow Convergence Regions in Adaptive
Systems**

by

Oscar Nouwens

B.Eng., University of Pretoria (2014)

Submitted to the Department of Mechanical Engineering
in partial fulfillment of the requirements for the degree of

Master of Science

at the

MASSACHUSETTS INSTITUTE OF TECHNOLOGY

June 2016

© Massachusetts Institute of Technology 2016. All rights reserved.



Signature redacted

Author

Department of Mechanical Engineering
May 16, 2016

Signature redacted

Certified by

Anuradha M. Annaswamy
Senior Research Scientist
Thesis Supervisor

Signature redacted

Accepted by

Rohan Abeyaratne
Chairman, Department Committee on Graduate Students

Analysis of Slow Convergence Regions in Adaptive Systems

by

Oscar Nouwens

Submitted to the Department of Mechanical Engineering
on May 16, 2016, in partial fulfillment of the
requirements for the degree of
Master of Science

Abstract

In this thesis, the convergence properties of errors are examined in a class of adaptive systems that corresponds to adaptive control of linear time-invariant plants with state variables accessible. The existence of a sticking region is demonstrated in the error space where the state errors move with a finite velocity independent of their magnitude. It is shown that these properties are also exhibited by adaptive systems with closed-loop reference models, which have been demonstrated to exhibit improved transient performance, as well as those that include an integral control in the inner-loop. Simulation and numerical studies are included to illustrate the size of this sticking region and its dependence on various system parameters. With the existence of sticking regions shown for inner-loop adaptive controllers, the impact on outer-loop control is demonstrated for systems that implement inner-loop adaptation.

Thesis Supervisor: Anuradha M. Annaswamy
Title: Senior Research Scientist

Acknowledgments

I would like to thank my advisor Dr. Anuradha Annaswamy, whose continued guidance and expertise allowed for great research progress and results. I would also like to thank Dr. Eugene Lavretsky of Boeing Research & Technology for his invaluable advise and suggestions. Thanks also to members of my research group, Daniel Wiese, Max Zheng Qu and Heather Hussain for their kind assistance and help during the course of my research. Finally, I would like to thank my Mom and Dad for their love and support during all these years.

THIS PAGE INTENTIONALLY LEFT BLANK

Contents

1	Introduction	13
2	Analysis of Sticking Regions	15
2.1	Problem Statement	16
2.1.1	The CRM-Adaptive System	16
2.1.2	The IC-Adaptive System	17
2.1.3	Slow Convergence Analysis	19
2.2	Analysis of the Sticking Region	19
2.2.1	Characterization of $x(t)$	20
2.2.2	Characterization of $x_m(t)$	23
2.2.3	Maximum Rate of Convergence During Sticking	25
2.2.4	Existence of Set \mathbf{S}	27
2.3	Simulation Study	30
2.4	Numerical Analysis	35
2.4.1	Numerical Results	36
2.4.2	Simulation Results	37
2.4.3	Additional Insight to Sticking in the IC-Adaptive System	39
2.5	Sticking Analysis with $(A, \lambda \mathbf{b})$ unknown	40
2.5.1	The CRM-Adaptive System with $(A, \lambda \mathbf{b})$ Unknown	41
2.5.2	Insight to Sticking in the CRM-Adaptive System with $(A, \lambda \mathbf{b})$ Un- known	42
2.5.3	Simulation Results	43
2.6	Summary	44

3	Sticking in Outer-Loop Control	45
3.1	Problem Statement	46
3.1.1	The Outer-Loop Control Problem with Unknown Inner-Loop Dynamics	46
3.1.2	Impact of Inner-Loop Sticking on Outer-Loop Control	48
3.2	Analysis of Sticking in Outer-Loop Control	48
3.2.1	Inner-Loop Sticking	48
3.2.2	Outer-Loop Sticking	49
3.3	Outer-Loop Altitude Control with Inner-Loop Adaptation	51
3.3.1	Control Problem Formulation	52
3.3.2	Open-Loop Reference Model Design	55
3.3.3	Adaptive Control Design	60
3.3.4	Simulation Study with Sticking Analysis	66
3.4	Summary	73
4	Concluding Remarks	75

List of Figures

2-1	$\tilde{x}(t)$ trajectory in \mathbf{N} with $t_1 = 0$ and $t_2 \cong 290$	32
2-2	$\tilde{\Theta}(t)$ trajectory in \mathbf{S} with $t_1 = 0$ and $t_2 \cong 290$	32
2-3	$x(t)$, $x_m(t)$, $\tilde{\Theta}(t)$ and $\ \dot{\tilde{\Theta}}(t)\ $ versus time	32
2-4	Set \mathbf{N} in x space, set \mathbf{S} and the lower bound of t_2 for varying k . Arrows denote increasing values of k	33
2-5	$\tilde{x}(t)$ trajectory in \mathbf{N} when $L = I_{2 \times 2}$ with $t_1 = 0$ and $t_2 \cong 2300$	33
2-6	$\tilde{\Theta}(t)$ trajectory in \mathbf{S} when $L = I_{2 \times 2}$ with $t_1 = 0$ and $t_2 \cong 2300$	34
2-7	$x(t)$, $x_m(t)$, $\tilde{\Theta}(t)$ and $\ \dot{\tilde{\Theta}}(t)\ $ versus time when $L = I_{2 \times 2}$	34
2-8	$\tilde{x}(t)$ trajectory in \mathbf{N} for persistent excitation with $t_1 = 0$ and $t_2 \cong 560$	34
2-9	$\tilde{\Theta}(t)$ trajectory in \mathbf{S} for persistent excitation with $t_1 = 0$ and $t_2 \cong 560$	35
2-10	$x(t)$, $x_m(t)$, $\tilde{\Theta}(t)$ and $\ \dot{\tilde{\Theta}}(t)\ $ versus time for persistent excitation	35
2-11	x^* and $\delta\theta_{max}^*$ for versus k with $n = 2 \rightarrow 6$ in the CRM-adaptive system	37
2-12	x^* and $\delta\theta_{max}^*$ for versus k with $n = 2 \rightarrow 6$ in the IC-adaptive system	37
2-13	Settling time T for various initial conditions of the CRM and IC-adaptive systems	39
2-14	Settling time T for various initial conditions of the CRM-adaptive systems with (A) and $(A, \lambda \mathbf{b})$ unknown	44
3-1	Open-loop plant with inner and outer-loop dynamics	47
3-2	Longitudinal flight angle relations [9]	53
3-3	Open-loop reference model block diagram	56
3-4	Pursuit based guidance algorithm [3]	58
3-5	Open-loop reference model pole-zero map and step response	60

3-6	Control architecture with error state feedback loops	62
3-7	Bode plots for the transfer functions from $e_x(s)$ to $x_g(s) - x_{gORM}(s)$	69
3-8	Altitude reponse $h(t)$, command signal $h_{cmd}(t)$ and elevator input $u(t)$ versus time for $k = 1$	70
3-9	Altitude reponse $h(t)$, command signal $h_{cmd}(t)$ and elevator input $u(t)$ versus time for $k = 10$	71
3-10	Inner-loop sticking in <i>Controller 1</i> and <i>Controller 2</i> for $t \in [0, 700]$ with $k = 10$	72
3-11	$\tilde{x}_{pm}(t)$ superimposed over \mathbf{N} for <i>Controller 1</i> and <i>Controller 2</i> for $t \in [0, 700]$ with $k = 10$	73
3-12	Altitude reponse $h(t)$, command signal $h_{cmd}(t)$ and elevator input $u(t)$ of <i>Controller 2</i> versus time for $k = 10$ and $t \in [0, 4000]$	73

List of Tables

3.1	Definitions for the inner-loop sticking analysis	50
3.2	Stability and control derivatives with uncertainties	55

THIS PAGE INTENTIONALLY LEFT BLANK

Chapter 1

Introduction

The stability of adaptive systems corresponding to the control of linear time-invariant plants has been well documented in the literature, with the tracking error converging to zero for any reference input [10]. If in addition, conditions of persistence of excitation are met, these adaptive systems can be shown to be uniformly asymptotically stable (u.a.s.) as well. Recently, in [8], it was shown that for low order plants, these adaptive systems cannot be shown to be exponentially stable, and are at best u.a.s. The main contribution of this thesis is the extension of this result to general linear time-invariant plants. Two classes of adaptive systems are considered both of which are shown to be u.a.s. and not exponentially stable, and are described in Chapters 2 and 3. The most important implication of the property of u.a.s. is the existence of a sticking region in the underlying error-state space where the trajectories move very slowly. This corresponds to places where the overall adaptive system is least robust. As a result, a precise characterization of this sticking region is important and is the main contribution of Chapter 2. Simulation and numerical results are included to complement the theoretical derivations.

In proving the existence of sticking regions, we show that the system will not only exhibit slow convergence of the state errors when traversing through the sticking region, but that the plant states will remain constrained in a well defined region during this time. This means that certain plant states are inaccessible during sticking which may have major implications for outer-loop controllers that implement inner-loop adaptation. This forms the scope of Chapter 3 which deals with analyzing the impact of inner-loop sticking regions

on outer-loop control. A complete example of an aircraft autopilot system for altitude control is included to illustrate the significance of sticking regions in a practical application.

Chapter 2

Analysis of Sticking Regions

In this chapter, two different types of adaptive controllers are considered. The first corresponds to the use of closed-loop reference models [5], [6], [13] (denoted as CRM-adaptive systems), and the second corresponds to the use of integral control for command tracking [9] (denoted as IC-adaptive systems). For both controllers, an analysis is presented that proves the existence of sticking regions for a general n^{th} order linear time-invariant plant, whose states are accessible. Later in the chapter, simulation results are provided to complement the theoretical derivations.

Consider the n^{th} order time-invariant plant differential equation is given by

$$\dot{x}(t) = Ax(t) + \mathbf{b}u(t). \quad (2.1)$$

By implementing adaptation, this plant may be controlled with a tracking error converging to zero when there are uncertainties in the system (A, \mathbf{b}) [10]. However, in this chapter, it is assumed that the input vector \mathbf{b} is constant and known such that all the uncertainty lies in the matrix A , which is constant. With this assumption, the complexity of the analysis is reduced. The case where there are additional uncertainties in \mathbf{b} is only briefly discussed at the end of this chapter using insights gained throughout the analysis. Simulations are also included for the case where \mathbf{b} is unknown, however, it is not the main focus of the chapter.

2.1 Problem Statement

We consider two classes of adaptive systems to demonstrate the region of slow convergence, the first of which is the CRM-adaptive system and second is the IC-adaptive system. For both systems, only the single input case is considered. In this section, we present the underlying adaptive systems and state the overall problem with regard to sticking regions. Throughout the analysis, it is assumed that the underlying reference input is bounded and smooth.

2.1.1 The CRM-Adaptive System

The n^{th} order time-invariant plant differential equation is given by

$$\dot{x}(t) = Ax(t) + \mathbf{b}u(t) \quad (2.2)$$

where A is a constant $n \times n$ unknown matrix and \mathbf{b} is a known vector of size n . A state variable feedback controller is defined by

$$u(t) = \Theta(t)x(t) + q^*r(t) \quad (2.3)$$

where $\Theta(t)$ is the time varying adaptive parameter updated as

$$\dot{\Theta}(t) = -\mathbf{b}^T P e(t) x^T(t). \quad (2.4)$$

Here $e(t) = x(t) - x_m(t)$ and $x_m(t)$ is the output of a reference model defined by

$$\dot{x}_m(t) = A_m x_m(t) + \mathbf{b}_m r(t) + L e(t) \quad (2.5)$$

where A_m is Hurwitz, $\mathbf{b}_m = q^* \mathbf{b}$, q^* is a known scalar and L is a constant $n \times n$ feedback matrix which introduces a closed-loop in the reference model. If $L = 0$, then (2.5) represents the open-loop reference model, denoted as the ORM adaptive system. With the standard

matching condition [10]

$$A + \mathbf{b}\Theta^* = A_m \quad (2.6)$$

satisfied, the error differential equation is defined by

$$\dot{e}(t) = [A_m - L]e(t) + \mathbf{b}\tilde{\Theta}(t)x(t) \quad (2.7)$$

where $\tilde{\Theta}(t) = \Theta(t) - \Theta^*$. If $[A_m - L]$ is Hurwitz, then a symmetric positive definite P exists that solves the well known Lyapunov equation

$$[A_m - L]^T P + P[A_m - L] = -Q_0 \quad (2.8)$$

where Q_0 is a symmetric positive definite matrix. It is well known that the error model in (2.7) and (2.4) can be shown to be globally stable at the origin and that [10]

$$\lim_{t \rightarrow \infty} e(t) = 0. \quad (2.9)$$

The goal in this analysis is to characterize regions in the $[e, \tilde{\Theta}]$ space where the speed of convergence is slow, i.e. identify the sticking region.

2.1.2 The IC-Adaptive System

The n_p^{th} order time-invariant plant differential equation is given by

$$\dot{x}_p(t) = A_p x_p(t) + \mathbf{b}_p u(t) \quad (2.10)$$

where A_p is a constant $n_p \times n_p$ unknown matrix and \mathbf{b}_p is a known vector of size n_p . The goal is to design a control input $u(t)$ such that the system output

$$y(t) = C_p x_p(t) \quad (2.11)$$

tracks a time-varying reference signal $r(t)$, where C_p is known and constant. An integral state e_{yI} is proposed as

$$e_{yI}(t) = \int_0^t [y(\tau) - r(\tau)] d\tau. \quad (2.12)$$

Augmenting (2.10) with the integrated output tracking error yields the n^{th} order extended plant differential equation given by

$$\dot{x}(t) = Ax(t) + \mathbf{b}u(t) + \mathbf{b}_m r(t) \quad (2.13)$$

where $x = [e_{yI}, x_p^T]^T$, $n = n_p + 1$ and

$$A = \begin{bmatrix} 0 & C_p \\ 0_{n_p \times 1} & A_p \end{bmatrix} \quad \mathbf{b} = \begin{bmatrix} 0 \\ \mathbf{b}_p \end{bmatrix} \quad \mathbf{b}_m = \begin{bmatrix} -1 \\ 0_{n_p \times 1} \end{bmatrix}. \quad (2.14)$$

A state variable feedback controller is defined by

$$u(t) = \Theta(t)x(t) \quad (2.15)$$

where $\Theta(t)$ is updated as

$$\dot{\Theta}(t) = -\mathbf{b}^T P e(t) x^T(t). \quad (2.16)$$

Here $e(t)$ is defined as in Section 2.1.1 and $x_m(t)$ is the output of a n^{th} reference model defined by

$$\dot{x}_m(t) = A_m x_m(t) + \mathbf{b}_m r(t) + L e(t) \quad (2.17)$$

where again, A_m is Hurwitz and L is a constant $n \times n$ feedback matrix. The matching condition and error differential equation are given as in (2.6) and (2.7) respectively, and the existence of a positive definite P that solves (2.8) is also guaranteed for a Hurwitz $[A_m - L]$. Using the same arguments as in the CRM-adaptive system, here too we can show that $\lim_{t \rightarrow \infty} e(t) = 0$. With this it can be shown that the control goal of interest may be reached [9]. The objective of this analysis is to characterize sticking regions in this IC-adaptive system, given by (2.13) through (2.17), in addition to those in the CRM-adaptive system.

2.1.3 Slow Convergence Analysis

From (2.4) and (2.16), it can be seen that the time varying adaptive gain $\Theta(t)$ is updated through the plant and reference model states only. This creates the premise for characterizing sticking regions as the update law has no dependence on the adaptive gain $\Theta(t)$ itself.

Our approach will be as follows: Determine a region \mathbf{S} in the $\tilde{\Theta}$ space, \mathbf{N} in the \tilde{x} space and \mathbf{R} in the x_m space. Here \tilde{x} is simply a deviation of the plant state from a fictitious trajectory as will be later defined. We continue our approach by showing that there are some initial conditions for which $\tilde{\Theta}(t)$ will remain in \mathbf{S} , $\tilde{x}(t)$ in \mathbf{N} and $x_m(t)$ in \mathbf{R} , over a certain interval, with $\|\tilde{\Theta}(t)\|$ remaining finite. The combined set

$$\mathcal{S} : \left\{ [\tilde{\Theta}, \tilde{x}, x_m] \in \mathbb{R}^{3n} \mid \tilde{\Theta} \in \mathbf{S}, \tilde{x} \in \mathbf{N}, x_m \in \mathbf{R} \right\} \quad (2.18)$$

is defined to be the sticking region. In the following section, we demonstrate the existence of this sticking region.

2.2 Analysis of the Sticking Region

In order to establish the sticking region, we need to guarantee the existence of a finite Θ_d^* such that

$$\|\dot{\tilde{\Theta}}(t)\| \leq \Theta_d^* \quad \forall t \in [t_1, t_2] \quad (2.19)$$

and a t_2 such that

$$t_2 - t_1 \geq \frac{\delta\theta^*}{\Theta_d^*} \quad (2.20)$$

where $\delta\theta^*$ is a lower bound defined as

$$\|\tilde{\Theta}(t_2) - \tilde{\Theta}(t_1)\| \geq \delta\theta^*. \quad (2.21)$$

The above implies that the parameter error moves slowly for all $t \in [t_1, t_2]$. In order to satisfy (2.19), we examine (2.4) and (2.16) and conditions under which $x(t)$ remains small. This

is addressed in Section 2.2.1 which follows. A similar procedure is adopted to characterize $x_m(t)$ in Section 2.2.2. With these characterizations, the sticking region \mathcal{S} as defined in (2.18), is analyzed in Section 2.2.3.

2.2.1 Characterization of $x(t)$

Using the matching condition in (2.6) and feedback controllers from (2.3) and (2.15), the plant differential equations for the CRM and IC-adaptive systems in (2.2) and (2.13), respectively, may be written similarly as

$$\dot{x}(t) = [A_m + \mathbf{b}\tilde{\Theta}(t)]x(t) + \mathbf{b}_m r(t) \quad (2.22)$$

with $\mathbf{b}_m = q^* \mathbf{b}$ for CRM-adaptive system and defined as (2.14) for the IC-adaptive system. We consider an arbitrary point Θ_0 , and a fictitious trajectory $\hat{x}(t)$ and the deviation $\tilde{x}(t)$ of $x(t)$ from $\hat{x}(t)$. That is, we define

$$\tilde{\Theta}(t) = \Theta_0 + \delta\tilde{\Theta}(t) \quad (2.23)$$

$$\hat{x}(t) = -[A_m + \mathbf{b}\Theta_0]^{-1} \mathbf{b}_m r(t) \quad (2.24)$$

$$\tilde{x}(t) = x(t) - \hat{x}(t). \quad (2.25)$$

Using equations (2.22) through (2.25), a differential equation for the state $\tilde{x}(t)$ may be expressed as

$$\dot{\tilde{x}}(t) = [A_m + \mathbf{b}\tilde{\Theta}(t)]\tilde{x}(t) + \mathbf{b}\delta\tilde{\Theta}(t)\hat{x}(t) - \dot{\hat{x}}(t). \quad (2.26)$$

If $\hat{A}(\tilde{\Theta}(t)) = [A_m + \mathbf{b}\tilde{\Theta}(t)]$ and $\mathbf{w}(t) = \mathbf{b}\delta\tilde{\Theta}(t)\hat{x}(t) - \dot{\hat{x}}(t)$, then the following linear time-variant plant differential equation is obtained:

$$\dot{\tilde{x}}(t) = \hat{A}(\tilde{\Theta}(t))\tilde{x}(t) + \mathbf{w}(t). \quad (2.27)$$

The following energy function of $\tilde{x}(t)$ will be used to examine the propensity of $\tilde{x}(t)$ towards 0:

$$V_{\tilde{x}}(t) = \tilde{x}^T(t)Y\tilde{x}(t) > 0 \quad \forall \tilde{x}(t) \neq 0 \quad (2.28)$$

where Y is a symmetric positive definite matrix. Additionally the sets are defined:

$$\mathbf{S} : \left\{ \tilde{\Theta} \in \mathbb{R}^n \mid \left[\hat{A}^T(\tilde{\Theta})Y + Y\hat{A}(\tilde{\Theta}) + I \right] < 0 \cap \right. \\ \left. \|\tilde{\Theta} - \Theta_0\| \leq \|Y\mathbf{b}\|^{-\alpha} \right\} \quad (2.29)$$

$$\mathbf{M} : \left\{ \tilde{x} \in \mathbb{R}^n \mid \|\tilde{x}\|^2 \geq 4\beta^2 \right\} \quad (2.30)$$

$$\mathbf{N} : \left\{ \tilde{x} \in \mathbb{R}^n \mid \tilde{x}^T Y \tilde{x} \leq 4\lambda_{\max}(Y)\beta^2 \right\} \quad (2.31)$$

where

$$\beta \geq \|(A_m + \mathbf{b}\Theta_0)^{-1}\mathbf{b}_m\| (\|Y\mathbf{b}\|^{1-\alpha} r^* + \|Y\|r_d^*). \quad (2.32)$$

Here $|r(t)| \leq r^* \forall t$, $|\dot{r}(t)| \leq r_d^* \forall t$ and α is a positive constant chosen as $0 \leq \alpha \leq 1$. Throughout this analysis, $\lambda_{\min}(B)$ and $\lambda_{\max}(B)$ will be used to denote the smallest and largest eigenvalues, respectively, of a matrix B .

It should be noted that \mathbf{M} is an unbounded region in \mathbb{R}^n outside a bounded sphere, while \mathbf{N} is a bounded ellipsoid. \mathbf{S} is a set in \mathbb{R}^n whose existence is yet to be demonstrated.

Lemma 1. *From the definition of \mathbf{M} and \mathbf{N} in (2.30) and (2.31) respectively, it follows that*

$$\mathbf{N}^c \subset \mathbf{M}.$$

Proof. From the definition of \mathbf{N} , it is known that

$$\lambda_{\max}(Y)\|\tilde{x}\|^2 \geq \tilde{x}^T Y \tilde{x} > 4\lambda_{\max}(Y)\beta^2 \quad \forall \tilde{x} \in \mathbf{N}^c \quad (2.33)$$

or simply

$$\|\tilde{x}\|^2 > 4\beta^2 \quad \forall \tilde{x} \in \mathbf{N}^c. \quad (2.34)$$

The bounds in (2.33) and (2.34) are well defined as Y is a symmetric positive definite matrix. From the definition of \mathbf{M} , equation (2.34) implies that $\mathbf{N}^c \subset \mathbf{M}$. \square

With the above definitions and properties, we demonstrate the propensity for $\tilde{x}(t)$ to remain in \mathbf{N} in the following theorem.

Theorem 2. If (i) $\tilde{\Theta}(t) \in \mathbf{S} \forall t \in [t_1, t_2]$ where $t_2 > t_1$, and (ii) $\tilde{x}(t_1) \in \mathbf{N}$, then

$$\tilde{x}(t) \in \mathbf{N} \forall t \in [t_1, t_2].$$

Proof. The time derivative of $V_{\tilde{x}}(t)$ in (2.28) is

$$\dot{V}_{\tilde{x}}(t) = \tilde{x}^T [\hat{A}^T(\tilde{\Theta}(t))Y + Y\hat{A}(\tilde{\Theta}(t))] \tilde{x} + 2\mathbf{w}^T(t)Y\tilde{x}. \quad (2.35)$$

From condition (i) in Theorem 2, equation (2.35) leads to the inequality

$$\dot{V}_{\tilde{x}}(t) < -\tilde{x}^T \tilde{x} + 2\mathbf{w}^T(t)Y\tilde{x} \quad (2.36)$$

for $t \in [t_1, t_2]$. Equation (2.36) may be rewritten as

$$\dot{V}_{\tilde{x}}(t) < -(\tilde{x} - Y\mathbf{w}(t))^T (\tilde{x} - Y\mathbf{w}(t)) + \|Y\mathbf{w}(t)\|^2. \quad (2.37)$$

From condition (i) in Theorem 2 and the definition of \mathbf{S} , it follows that

$$\|\delta\tilde{\Theta}(t)\| \leq \frac{1}{\|Y\mathbf{b}\|^\alpha} \forall t \in [t_1, t_2]. \quad (2.38)$$

From this, an upper bound on $\|Y\mathbf{w}(t)\|$ is determined for $t \in [t_1, t_2]$:

$$\begin{aligned} \|Y\mathbf{w}(t)\| &\leq \|Y\mathbf{b}\| \|\delta\tilde{\Theta}(t)\| \|(A_m + \mathbf{b}\Theta_0)^{-1} \mathbf{b}_m\| r^* + \\ &\quad \|Y\| \|(A_m + \mathbf{b}\Theta_0)^{-1} \mathbf{b}_m\| r_d^* \\ &\leq \|(A_m + \mathbf{b}\Theta_0)^{-1} \mathbf{b}_m\| (\|Y\mathbf{b}\|^{1-\alpha} r^* + \|Y\| r_d^*) \\ &\leq \beta. \end{aligned} \quad (2.39)$$

From (2.37), (2.39) and the definition of \mathbf{M} , it follows that for $t \in [t_1, t_2]$, $\dot{V}_{\tilde{x}}(t) < 0$ if $\tilde{x}(t) \in \mathbf{M}$ and condition (i) in Theorem 2 holds. From Lemma 1, this in turn implies that if conditions (i) and (ii) in Theorem 2 hold, then $\tilde{x}(t) \in \mathbf{N} \forall t \in [t_1, t_2]$. \square

2.2.2 Characterization of $x_m(t)$

The update laws in (2.4) and (2.16) are also affected by the reference model and thus it is important to characterize $x_m(t)$. The reference models for the CRM and IC-adaptive controllers may be written as

$$\dot{x}_m(t) = [A_m - L]x_m(t) + \mathbf{z}(t) \quad (2.40)$$

where $\mathbf{z}(t) = \mathbf{b}_m r(t) + Lx(t)$. Similar to the approach used to characterize $x(t)$, the following energy function of $x_m(t)$ will be used:

$$V_{x_m}(t) = x_m^T(t)Wx_m(t) > 0 \quad \forall x_m(t) \neq 0 \quad (2.41)$$

where

$$[A_m - L]^T W + W [A_m - L] = -I. \quad (2.42)$$

Since $[A_m - L]$ is Hurwitz, W is a symmetric positive definite matrix. Finally, sets \mathbf{Q} and \mathbf{R} are defined:

$$\mathbf{Q} : \left\{ x_m \in \mathbb{R}^n \mid \|x_m\|^2 \geq 4\Lambda^2 \right\} \quad (2.43)$$

$$\mathbf{R} : \left\{ x_m \in \mathbb{R}^n \mid x_m^T W x_m \leq 4\lambda_{\max}(W)\Lambda^2 \right\} \quad (2.44)$$

where

$$\Lambda > \|W\| (\|\mathbf{b}_m\| r^* + \|L\| x^*) \quad (2.45)$$

and

$$x^* = 2\beta \left(\frac{\lambda_{\max}(Y)}{\lambda_{\min}(Y)} \right)^{\frac{1}{2}} + \|(A_m + \mathbf{b}\Theta_0)^{-1} \mathbf{b}_m\| r^*. \quad (2.46)$$

Lemma 3. *From the definition of \mathbf{Q} and \mathbf{R} in (2.43) and (2.44) respectively, it follows that*

$$\mathbf{R}^c \subset \mathbf{Q}.$$

Proof. From the definition of \mathbf{R} , it is known that

$$\lambda_{\max}(W) \|x_m\|^2 \geq x_m^T W x_m > 4\lambda_{\max}(W)\Lambda^2 \quad \forall x_m \in \mathbf{R}^c \quad (2.47)$$

or simply

$$\|x_m\|^2 > 4\Lambda^2 \quad \forall x_m \in \mathbf{R}^c. \quad (2.48)$$

The bounds in (2.47) and (2.48) are well defined as W is a symmetric positive definite matrix. From the definition of \mathbf{Q} , equation (2.47) implies that $\mathbf{R}^c \subset \mathbf{Q}$. \square

As in the characterization of $x(t)$, we use the above definitions and properties to demonstrate the propensity for $x_m(t)$ to remain in \mathbf{R} in the following theorem.

Theorem 4. *If (i) $\tilde{x}(t) \in \mathbf{N} \quad \forall t \in [t_1, t_2]$ and (ii) $x_m(t_1) \in \mathbf{R}$, then*

$$x_m(t) \in \mathbf{R} \quad \forall t \in [t_1, t_2].$$

Proof. The time derivative of $V_{x_m}(t)$ in (2.41) is

$$\dot{V}_{x_m}(t) = -x_m^T x_m + 2\mathbf{z}^T(t) W x_m \quad (2.49)$$

which may also be expressed as

$$\dot{V}_{x_m}(t) = -(x_m - W\mathbf{z}(t))^T (x_m - W\mathbf{z}(t)) + \|W\mathbf{z}(t)\|^2. \quad (2.50)$$

From condition (i) in Theorem 4 and the definition of \mathbf{N} it follows that

$$\|\tilde{x}(t)\| \leq 2\beta \left(\frac{\lambda_{\max}(Y)}{\lambda_{\min}(Y)} \right)^{\frac{1}{2}} \quad \forall t \in [t_1, t_2]. \quad (2.51)$$

The bound in (2.51) is well defined as Y is a symmetric positive definite matrix. From the

inequality in (2.51) and the definition of \tilde{x} in (2.25), it follows that

$$\|x(t)\| \leq x^* \quad \forall t \in [t_1, t_2]. \quad (2.52)$$

From this, an upper bound on $\|Wz(t)\|$ is determined for $t \in [t_1, t_2]$:

$$\begin{aligned} \|Wz(t)\| &\leq \|W\| \|\mathbf{b}_m r(t) + Lx(t)\| \\ &\leq \|W\| (\|\mathbf{b}_m\| r^* + \|L\| x^*) \\ &< \Lambda. \end{aligned} \quad (2.53)$$

From (2.50), (2.53) and the definition of \mathbf{Q} , it follows that for $t \in [t_1, t_2]$, $\dot{V}_{x_m}(t) < 0$ if $x_m(t) \in \mathbf{Q}$. From Lemma 3, this in turn implies that if conditions (i) and (ii) in Theorem 4 hold, then $x_m(t) \in \mathbf{R} \quad \forall t \in [t_1, t_2]$. \square

2.2.3 Maximum Rate of Convergence During Sticking

Theorems 2 and 4 create the basis for analyzing sticking in the adaptive systems. That is, we determine conditions under which the parameter error $\tilde{\Theta}(t)$ has a bounded derivative, over a certain time interval. This is presented in the following theorem.

Theorem 5. *Let*

$$\Theta_d^* = \|\mathbf{b}^T P\| \left(x^{*2} + 2x^* \Lambda \left(\frac{\lambda_{\max}(W)}{\lambda_{\min}(W)} \right)^{\frac{1}{2}} \right). \quad (2.54)$$

If (i) $\tilde{\Theta}(t) \in \mathbf{S} \quad \forall t \in [t_1, t_2]$ where

$$t_2 = \min \{ t \mid \tilde{\Theta}(t_1) \in \mathbf{S}, \tilde{\Theta}(t + \delta t) \notin \mathbf{S} \quad \forall \delta t > 0, t > t_1 \}, \quad (2.55)$$

(ii) $\tilde{x}(t_1) \in \mathbf{N}$ and (iii) $x_m(t_1) \in \mathbf{R}$, then

$$t_2 - t_1 \geq \frac{\|\tilde{\Theta}(t_2) - \tilde{\Theta}(t_1)\|}{\Theta_d^*}. \quad (2.56)$$

Proof. From Theorem 2 and conditions (i) and (ii) of Theorem 5, it follows that $\tilde{x}(t) \in$

$\mathbf{N} \forall t \in [t_1, t_2]$. From Theorem 4, this in turn implies that if condition (iii) of Theorem 5 also holds, then $x_m(t) \in \mathbf{R} \forall t \in [t_1, t_2]$.

From the definition of \mathbf{N} and \mathbf{R} it follows that

$$\|\tilde{x}(t)\| \leq 2\beta \left(\frac{\lambda_{\max}(Y)}{\lambda_{\min}(Y)} \right)^{\frac{1}{2}} \forall t \in [t_1, t_2] \quad (2.57)$$

and

$$\|x_m(t)\| \leq 2\Lambda \left(\frac{\lambda_{\max}(W)}{\lambda_{\min}(W)} \right)^{\frac{1}{2}} \forall t \in [t_1, t_2]. \quad (2.58)$$

From the inequality in (2.57) and the definition of \tilde{x} in (2.25), it follows that

$$\|x(t)\| \leq x^* \forall t \in [t_1, t_2]. \quad (2.59)$$

An upper bound on $\tilde{\Theta}(t)$ for $t \in [t_1, t_2]$ can now be determined as

$$\begin{aligned} \|\dot{\tilde{\Theta}}(t)\| &= \|-\mathbf{b}^T P(x(t) - x_m(t))x^T(t)\| \\ &\leq \|\mathbf{b}^T P\| (\|x(t)\| \|x^T(t)\| + \|x_m(t)\| \|x^T(t)\|) \\ &\leq \|\mathbf{b}^T P\| \left(x^{*2} + 2x^* \Lambda \left(\frac{\lambda_{\max}(W)}{\lambda_{\min}(W)} \right)^{\frac{1}{2}} \right) \\ &= \Theta_d^*. \end{aligned}$$

This proves Theorem 5. □

Theorem 5 is the main result of this chapter. It establishes a lower bound on the duration of the time interval $[t_1, t_2]$ that is dependent on the maximum speed of convergence Θ_d^* and the size of set \mathbf{S} . The term “sticking region” was first used in [8] to describe a set in state space where the state rate remained bounded for a minimum time. This implies that the combined set \mathcal{S} in (2.18) is the *sticking region* with *sticking* occurring over the interval $[t_1, t_2]$ during which $\tilde{\Theta}(t) \in \mathbf{S}$, $\tilde{x}(t) \in \mathbf{N}$ and $x_m(t) \in \mathbf{R}$.

The conditions under which the lower bound of t_2 in (2.56) may be made arbitrarily large are investigated next. In order to determine these conditions, we first argue that \mathbf{S} as defined above exists.

2.2.4 Existence of Set \mathbf{S}

To establish the existence of \mathbf{S} , we first choose the symmetric matrix Y defined in (2.28).

For this purpose we define

$$\hat{A}_0 = A_m + \mathbf{b}\Theta_0 \quad (2.60)$$

where it is assumed that Θ_0 is such that \hat{A}_0 is Hurwitz. A symmetric and positive definite matrix \bar{Y} may therefore be defined by

$$\hat{A}_0^T \bar{Y} + \bar{Y} \hat{A}_0 = -I. \quad (2.61)$$

We now define Y using \bar{Y} in (2.61) and a positive constant γ^2 as

$$Y = (1 + \gamma^2) \bar{Y}. \quad (2.62)$$

The motivation for this selection of Y will become clear in the following theorem that proves the existence of \mathbf{S} :

Theorem 6. *Let*

$$\hat{A}_0 = A_m + \mathbf{b}\Theta_0 \quad (2.63)$$

be Hurwitz. Then \mathbf{S} exists and may be defined as

$$\mathbf{S} : \left\{ \tilde{\Theta} \in \mathbb{R}^n \mid -\delta\Theta^* \leq \tilde{\Theta} - \Theta_0 \leq \delta\Theta^* \right\} \quad (2.64)$$

where

$$\delta\Theta^* = [\delta\theta^*, \delta\theta^* \dots \delta\theta^*] \quad (2.65)$$

with

$$0 < \delta\theta^* < \min \left\{ \frac{\gamma^2}{2n\|Y\mathbf{b}\|_{max}}, \frac{1}{n\|Y\mathbf{b}\|^\alpha} \right\}. \quad (2.66)$$

Proof. Let

$$\mathbf{S}_1 : \left\{ \tilde{\Theta} \in \mathbb{R}^n \mid [\hat{A}^T(\tilde{\Theta})Y + Y\hat{A}(\tilde{\Theta}) + I] < 0 \right\} \quad (2.67)$$

$$\mathbf{S}_2 : \left\{ \tilde{\Theta} \in \mathbb{R}^n \mid \|\tilde{\Theta} - \Theta_0\| \leq \|Y\mathbf{b}\|^{-\alpha} \right\}. \quad (2.68)$$

It is easy to note that

$$\mathbf{S} \in \mathbf{S}_1 \cap \mathbf{S}_2. \quad (2.69)$$

We first show the existence of \mathbf{S}_1 . Since $\hat{A}(\tilde{\Theta})$ can be written as

$$\hat{A}(\tilde{\Theta}) = \hat{A}_0 + \mathbf{b}\delta\tilde{\Theta} \quad (2.70)$$

and \hat{A}_0 is Hurwitz, we use (2.61) and (2.62) to rewrite (2.67) as

$$\mathbf{S}_1 : \left\{ \tilde{\Theta} \in \mathbb{R}^n \mid C(\delta\tilde{\Theta}) < 0 \right\} \quad (2.71)$$

where

$$C(\delta\tilde{\Theta}) = [c_{ij}(\delta\tilde{\Theta})] = \delta\tilde{\Theta}^T \mathbf{b}^T Y + Y\mathbf{b}\delta\tilde{\Theta} - \gamma^2 I. \quad (2.72)$$

By considering diagonal dominance, it is known that $C(\delta\tilde{\Theta}) < 0$ if [2]

$$c_{ii}(\delta\tilde{\Theta}) < 0 \quad \forall i \quad (2.73)$$

and

$$|c_{ii}(\delta\tilde{\Theta})| > \sum_{j \neq i} |c_{ij}(\delta\tilde{\Theta})| \quad \forall i. \quad (2.74)$$

We will show that \mathbf{S}_1 in (2.71) exists by demonstrating that the elements of $C(\delta\tilde{\Theta})$ in (2.72) satisfy (2.73) and (2.74). By defining

$$\begin{aligned} c^* &= 2\|Y\mathbf{b}\|_{\max} \|\delta\tilde{\Theta}\|_{\max} \\ &\geq \|\delta\tilde{\Theta}^T \mathbf{b}^T Y + Y\mathbf{b}\delta\tilde{\Theta}\|_{\max} \end{aligned} \quad (2.75)$$

it is known that

$$c_{ii}(\delta\tilde{\Theta}) \leq c^* - \gamma^2 \quad \forall i \quad (2.76)$$

and

$$(n-1)c^* \geq \sum_{j \neq i} |c_{ij}(\delta\tilde{\Theta})| \quad \forall i. \quad (2.77)$$

By utilizing inequalities (2.76) and (2.77), conditions (2.73) and (2.74) become

$$c_{ii}(\delta\tilde{\Theta}) \leq c^* - \gamma^2 < 0 \quad \forall i \quad (2.78)$$

and

$$\begin{aligned} |c_{ii}(\delta\tilde{\Theta})| &> (n-1)c^* \\ &\geq \sum_{j \neq i} |c_{ij}(\delta\tilde{\Theta})| \quad \forall i. \end{aligned} \quad (2.79)$$

Both conditions (2.78) and (2.79) may be satisfied if

$$c^* < \frac{\gamma^2}{n} \quad (2.80)$$

or equivalently

$$\|\delta\tilde{\Theta}\|_{max} \leq \frac{\gamma^2}{2n\|Y\mathbf{b}\|_{max}}. \quad (2.81)$$

Thus, set \mathbf{S}_1 is defined in $\tilde{\Theta}$ space where (2.81) is satisfied. We now consider the existence of \mathbf{S}_2 . Since

$$\|\tilde{\Theta} - \Theta_0\| \leq n\|\delta\tilde{\Theta}\|_{max}, \quad (2.82)$$

the set \mathbf{S}_2 is well defined if

$$\|\delta\tilde{\Theta}\|_{max} \leq \frac{1}{n\|Y\mathbf{b}\|_{\alpha}}. \quad (2.83)$$

The definition of \mathbf{S} in (2.64) describes an admissible set such that the conditions for set \mathbf{S}_1 and \mathbf{S}_2 in (2.81) and (2.83) respectively, are satisfied for all $\tilde{\Theta} \in \mathbf{S}$. \square

The existence of set \mathbf{S} has now been shown under the condition that \hat{A}_0 in (2.63) is Hurwitz. Each Θ_0 that satisfies this condition describes a certain set \mathbf{S} . It will become clear from the simulation results that the selection of Θ_0 greatly effects sticking if $\tilde{\Theta}(t_1) = \Theta_0$.

2.3 Simulation Study

We carry out simulations in this section to describe the sticking region \mathcal{S} . A second order plant and reference model are chosen as in (2.2) and (2.5) with

$$A = \begin{bmatrix} 0 & 1 \\ -4 & 4 \end{bmatrix} \quad \mathbf{b} = \begin{bmatrix} 0 \\ 1 \end{bmatrix} \quad (2.84)$$

$$A_m = \begin{bmatrix} 0 & 1 \\ -1 & -2 \end{bmatrix} \quad \mathbf{b}_m = \mathbf{b} \quad L = \begin{bmatrix} 0 & 0 \\ 0 & 0 \end{bmatrix}. \quad (2.85)$$

An adaptive controller as in (2.3) and (2.4) was simulated where P in (2.4) was solved using (2.8) with $Q_0 = I$. A constant reference input was chosen with $r(t) = 1$. In order to define a set \mathbf{S} , we use Theorem 6 which requires \hat{A}_0 in (2.63) to be Hurwitz. By setting $\Theta_0 = [-24, -24]$, the following eigenvalues of \hat{A}_0 are obtained:

$$\lambda_1(\hat{A}_0) = -1 \quad \lambda_2(\hat{A}_0) = -25. \quad (2.86)$$

With \hat{A}_0 known, we can define \tilde{Y} and Y using (2.61) and (2.62) with $\gamma = 1$. We use (2.32) and (2.45) to set β and Λ , respectively, as small as possible with

$$\beta = 0.04 \quad \Lambda = 1.71. \quad (2.87)$$

\mathbf{S} is then defined in (2.64) with $\delta\theta^* = 6.25$ set as large as possible in (2.66) with $\alpha = 1$. Following the definitions in (2.31) and (2.44), the sets \mathbf{N} and \mathbf{R} are defined. The sticking

region \mathcal{S} is then given by (2.18) with

$$\begin{aligned} \mathbf{S} &: \left\{ \tilde{\Theta} \in \mathbb{R}^2 \mid - \begin{bmatrix} 6.25 \\ 6.25 \end{bmatrix}^T \leq \tilde{\Theta} + \begin{bmatrix} 24 \\ 24 \end{bmatrix}^T \leq \begin{bmatrix} 6.25 \\ 6.25 \end{bmatrix}^T \right\} \\ \mathbf{N} &: \left\{ \tilde{x} \in \mathbb{R}^2 \mid \tilde{x}^T \begin{bmatrix} 2.04 & 0.04 \\ 0.04 & 0.04 \end{bmatrix} \tilde{x} \leq 0.013 \right\} \\ \mathbf{R} &: \left\{ x_m \in \mathbb{R}^2 \mid x_m^T \begin{bmatrix} 1.5 & 0.5 \\ 0.5 & 0.5 \end{bmatrix} x_m \leq 19.90 \right\}. \end{aligned}$$

We choose the initial conditions at $t_1 = 0$ as

$$\tilde{\Theta}(t_1) = \Theta_0 \quad \tilde{x}(t_1) = 0 \quad x_m(t_1) = -A_m^{-1} \mathbf{b}_m r(t_1). \quad (2.88)$$

That is, the system trajectory begins in \mathcal{S} and the conditions of Theorem 5 are satisfied. From (2.54), we compute Θ_d^* to be 3.87. Finally, using (2.56), we compute the lower bound on t_2 using the values of Θ_d^* and $\delta\theta^*$ as

$$t_2 \geq 1.61. \quad (2.89)$$

In order to validate this analytical prediction, a numerical simulation of the CRM-adaptive system specified by (2.84), (2.85) and (2.88) was carried out, the results of which are shown in Figures 2-1 to 2-3. It can be seen from these figures that $\tilde{x}(t) \in \mathbf{N}$, $\tilde{\Theta}(t) \in \mathbf{S}$ and $\|\dot{\tilde{\Theta}}(t)\| \leq \Theta_d^* \forall t \in [0, 290]$. This confirms (2.89).

The lower bound of $t_2 \geq 1.61$ from (2.89) may mislead the reader into thinking that the sticking may occur only for a short period of time. This is not true; it should be noted that the selection of Θ_0 above was done arbitrarily, insuring only that \hat{A}_0 was Hurwitz. Suppose that Θ_0 is chosen such that the eigenvalues of \hat{A}_0 are set as follows:

$$\lambda_1(\hat{A}_0) = -1 \quad \lambda_2(\hat{A}_0) = -k \quad \text{with } k > 1. \quad (2.90)$$

Repeating the same procedure as above for the \hat{A}_0 as in (2.90), \mathbf{N} and \mathbf{S} as well as the lower

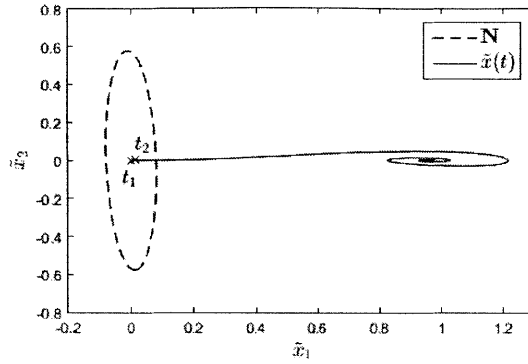


Figure 2-1: $\tilde{x}(t)$ trajectory in N with $t_1 = 0$ and $t_2 \cong 290$

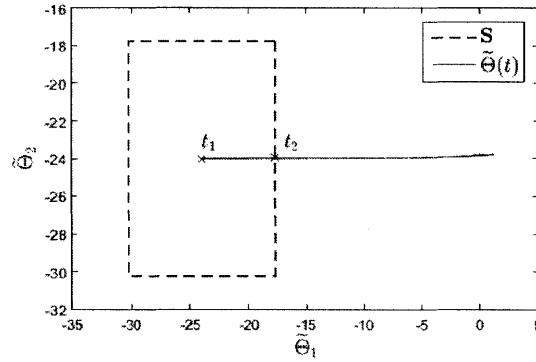


Figure 2-2: $\tilde{\Theta}(t)$ trajectory in S with $t_1 = 0$ and $t_2 \cong 290$

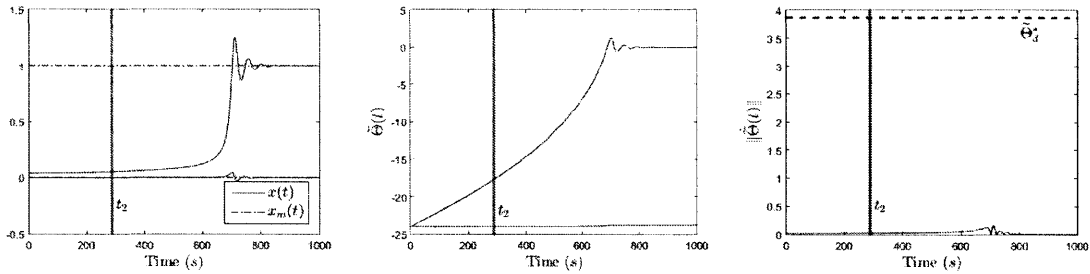


Figure 2-3: $x(t)$, $x_m(t)$, $\tilde{\Theta}(t)$ and $\|\tilde{\Theta}(t)\|$ versus time

bound on t_2 can be calculated. These are shown in Figure 2-4, which clearly illustrates that as initial condition increases in magnitude, the time that the trajectories spend in the sticking region grows as well. Here the effects of sticking become predominant in the CRM-adaptive system as Θ_d^* may be made arbitrarily small by increasing k . This is due to a decreasing size of N about $x = 0$ and increasing size of S when k is increased.

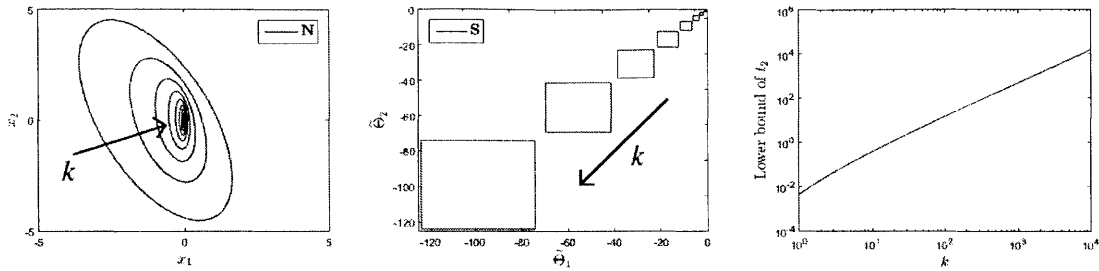


Figure 2-4: Set \mathbf{N} in x space, set \mathbf{S} and the lower bound of t_2 for varying k . Arrows denote increasing values of k

In Section 2.4 which follows, we extend the observation in Figure 2-4 to general n^{th} order systems. However, let us first consider some additional simulations. In (2.85) we let $L = 0$ such that no closed-loop reference model was defined. In [5], [6], it has been demonstrated that adaptive systems with closed-loop reference models exhibit improved transient performance. We therefore suspect that introducing the error state feedback may improve the transient performance during sticking. The simulation as presented in (2.84) though (2.88) is repeated for the case when $L = I_{2 \times 2}$. The results are shown in Figures 2-5 through 2-7. It can be seen from these figures that $\tilde{x}(t) \in \mathbf{N}$, $\tilde{\Theta}(t) \in \mathbf{S}$ and $\|\dot{\tilde{\Theta}}(t)\| \leq \Theta_d^* \forall t \in [0, 2300]$. We observe that the new feedback L has reduced Θ_d^* which has made the system more susceptible to sticking.

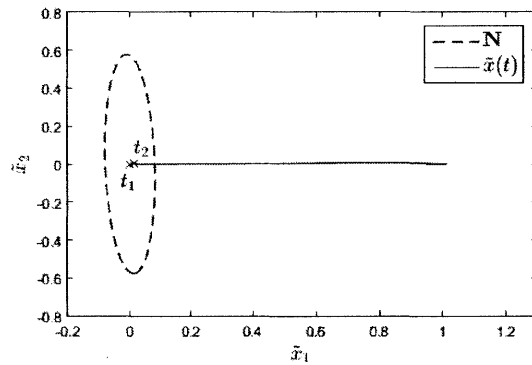


Figure 2-5: $\tilde{x}(t)$ trajectory in \mathbf{N} when $L = I_{2 \times 2}$ with $t_1 = 0$ and $t_2 \approx 2300$

Finally, let us consider the case for when the conditions of persistent excitation are satisfied. Once again, we repeat the simulation as presented in (2.84) though (2.88), but define $r(t) = \sin(2\pi t/200)$ such that persistent excitation is achieved. The results are shown in

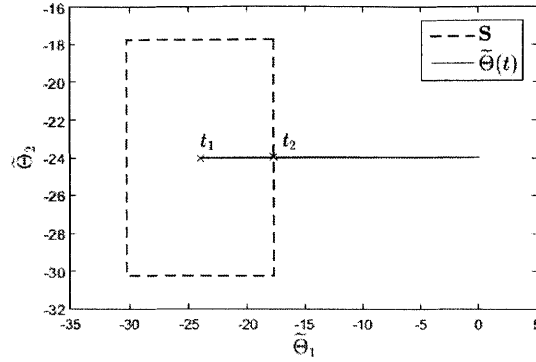


Figure 2-6: $\tilde{\Theta}(t)$ trajectory in S when $L = I_{2 \times 2}$ with $t_1 = 0$ and $t_2 \approx 2300$

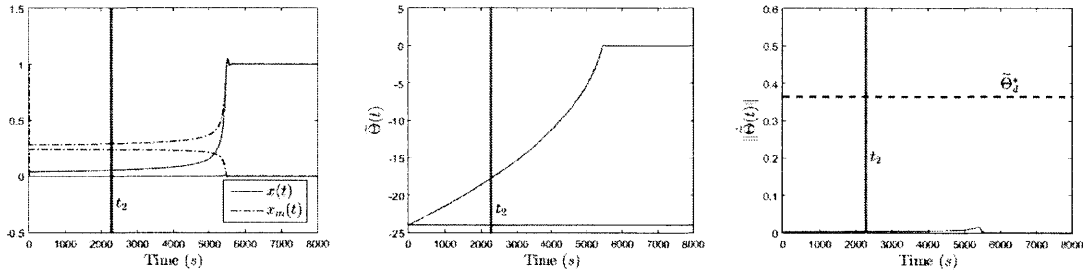


Figure 2-7: $x(t)$, $x_m(t)$, $\tilde{\Theta}(t)$ and $\|\tilde{\Theta}(t)\|$ versus time when $L = I_{2 \times 2}$

Figures 2-8 through 2-10. Here the response is only plotted until shortly after the system leaves the sticking region and $\tilde{x}_m(t) = x_m(t) - \hat{x}(t)$. It can be seen from these figures that $\tilde{x}(t) \in N$ and $\tilde{\Theta}(t) \in S \forall t \in [0, 560]$. Thus persistent excitation does not make the system less susceptible to sticking.

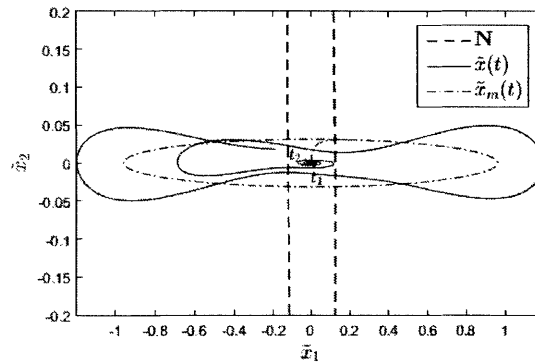


Figure 2-8: $\tilde{x}(t)$ trajectory in N for persistent excitation with $t_1 = 0$ and $t_2 \approx 560$

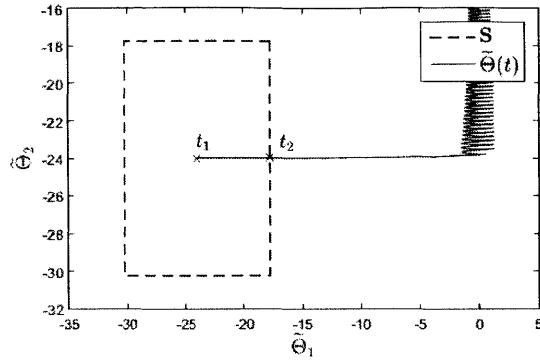


Figure 2-9: $\tilde{\Theta}(t)$ trajectory in S for persistent excitation with $t_1 = 0$ and $t_2 \cong 560$

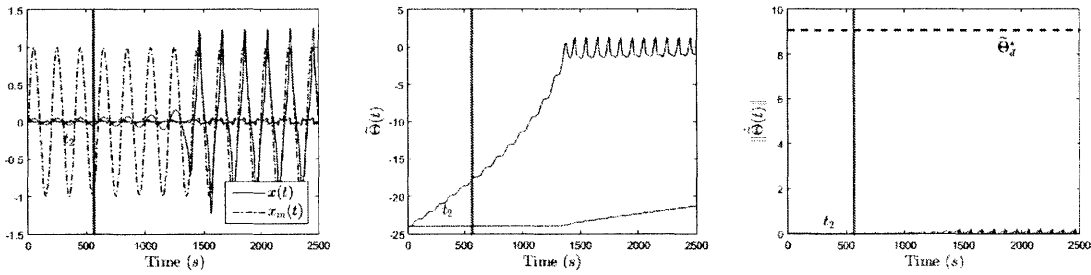


Figure 2-10: $x(t)$, $x_m(t)$, $\tilde{\Theta}(t)$ and $\|\tilde{\Theta}(t)\|$ versus time for persistent excitation

2.4 Numerical Analysis

In this section, we address the lower bound on t_2 , from Theorem 5, and its dependence on initial conditions for general n^{th} order CRM and IC-adaptive systems. In order to do this, it is assumed that (A, \mathbf{b}) is expressed in control canonical form such that

$$A = \begin{bmatrix} 0 & & & \\ \vdots & & I & \\ a_1 & a_2 & \cdots & a_n \end{bmatrix} \quad \mathbf{b} = \begin{bmatrix} 0 \\ \vdots \\ 0 \\ 1 \end{bmatrix}. \quad (2.91)$$

This is possible for the CRM-adaptive plant defined in (2.2) since up to this point, no constraints have been placed on the system (A, \mathbf{b}) . However, the IC-adaptive plant is defined according to the augmentation in (2.14). It is clear that if $C_p = [1 \ 0 \ \cdots \ 0]$ in (2.11) and (A_p, \mathbf{b}_p) is represented in control canonical form in (2.10), then (A, \mathbf{b}) in (2.14) is

similar to (2.91) with $a_1 = 0$. This is the case considered in this section.

By representing both the CRM and IC-adaptive systems in control canonical form, we are able to closely compare the numerical results that follow in the next section.

2.4.1 Numerical Results

For a system that is initialized in the sticking region with $\tilde{\Theta}(t_1) = \Theta_0$, we have from Theorem 5 and 6 that

$$t_2 - t_1 \geq \frac{\|\tilde{\Theta}(t_2) - \tilde{\Theta}(t_1)\|}{\Theta_d^*} \geq \frac{\delta\theta^*}{\Theta_d^*}. \quad (2.92)$$

For any given adaptive system, it is clear from (2.45) and (2.54) that if x^* (defined in (2.46)) decreases, then Θ_d^* in (2.92) will decrease provided Λ is always set to the lower bound in (2.45). Additionally, by considering (2.66), $\delta\theta^*$ may be increased if the upper bound

$$\delta\theta_{max}^* = \min \left\{ \frac{\gamma^2}{2n\|Y\mathbf{b}\|_{max}}, \frac{1}{n\|Y\mathbf{b}\|^\alpha} \right\} \quad (2.93)$$

increases. Therefore, in order to determine the conditions under which the lower bound on t_2 in (2.92) may be made arbitrarily large, only the quantities x^* and $\delta\theta_{max}^*$ need to be analyzed. This will be the approach used in the remainder of this section.

In these numerical results, it is assumed that the reference input is constant such that $r^* = 1$ and $r_d^* = 0$. In order to define a set \mathbf{S} , we choose Θ_0 in (2.63) such that

$$\begin{aligned} \lambda_i(\hat{A}_0) &= -1 \quad \text{for } i = 1 \dots n-1 \\ \lambda_n(\hat{A}_0) &= -k \quad \text{with } k > 1. \end{aligned} \quad (2.94)$$

We now define \bar{Y} and Y using (2.61) and (2.62) with $\gamma = 1$. β is then defined as the lower bound in (2.32) with $\alpha = 1$ and $\alpha = 0.3$, respectively, for the CRM and IC-adaptive systems. By setting Λ to the lower bound in (2.45), we show how x^* and $\delta\theta_{max}^*$ vary with k in Figure 2-11 for the CRM-adaptive system and Figure 2-12 for the IC-adaptive system. In these figures, results for system orders from two to six are shown.

It is clear from these graphs that the lower bound of t_2 in (2.92) may be made arbitrarily large for the CRM and IC-adaptive systems. However, the lower bound grows more rapidly

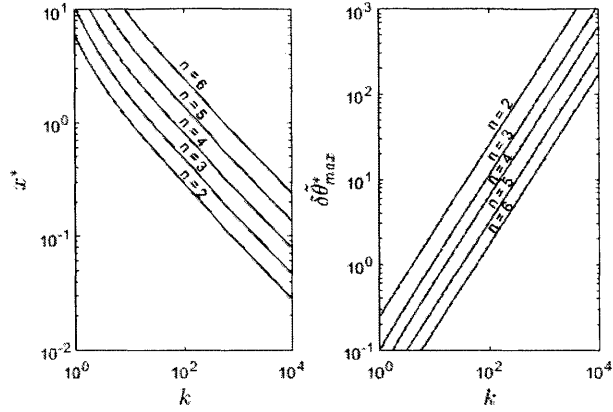


Figure 2-11: x^* and $\delta\theta_{max}^*$ for versus k with $n = 2 \rightarrow 6$ in the CRM-adaptive system

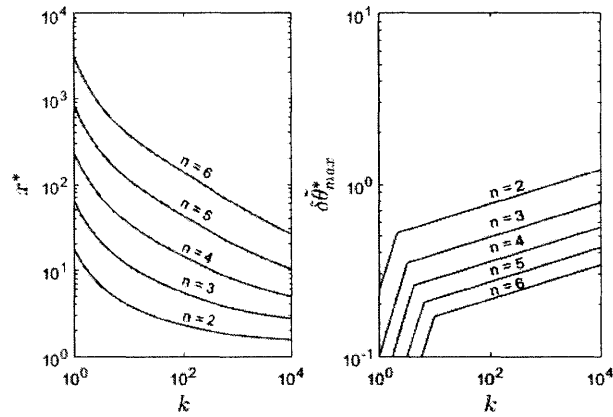


Figure 2-12: x^* and $\delta\theta_{max}^*$ for versus k with $n = 2 \rightarrow 6$ in the IC-adaptive system

for the CRM-adaptive system. Additionally, it can be seen that x^* approaches a non-zero value as k increases for the IC-adaptive system, while x^* approaches zero for the CRM-adaptive system. This means that Θ_d^* may be made arbitrarily small by increasing k for the CRM-adaptive system, but not for the IC-adaptive system.

2.4.2 Simulation Results

To illustrate sticking and the significance of Figures 2-11 and 2-12, simulations were carried out for a CRM and IC-adaptive system defined in Section 2.1.1 and 2.1.2, respectively,

by

$$A = \begin{bmatrix} 0 & 1 & 0 \\ 0 & 0 & 1 \\ 0 & -4 & -4 \end{bmatrix} \quad \mathbf{b} = \begin{bmatrix} 0 \\ 0 \\ 1 \end{bmatrix} \quad (2.95)$$

$$A_m = \begin{bmatrix} 0 & 1 & 0 \\ 0 & 0 & 1 \\ -1 & -3 & -3 \end{bmatrix} \quad L = \begin{bmatrix} 0_{3 \times 3} \end{bmatrix} \quad (2.96)$$

with $\mathbf{b}_m = \mathbf{b}$ for CRM-adaptive system and defined in (2.14) for the IC-adaptive system. For the CRM-adaptive system, an adaptive controller as in (2.3) and (2.4) was simulated where P in (2.4) was solved using (2.8) with $Q_0 = I$. For the IC-adaptive system, an adaptive controller as in (2.15) and (2.16) was simulated with the same P . A constant reference input was chosen with $r(t) = 1$ and the system was initialized at $t_1 = 0$ as

$$x(t_1) = 0 \quad x_m(t_1) = 0 \quad \tilde{\Theta}(t_1) = [\tilde{\theta}_0, \tilde{\theta}_0, \tilde{\theta}_0]. \quad (2.97)$$

For each simulation, the initial conditions in (2.97) were used for increasingly negative values of $\tilde{\theta}_0$ while recording the settling time T defined as

$$T = \min \left\{ t \mid \frac{\|z(t) - z^*\|}{\|z(t_1) - z^*\|} < \varepsilon \right\} \quad (2.98)$$

where $z(t) = [x(t), x_m(t), \tilde{\Theta}(t)]^T$, $z^* = \lim_{t \rightarrow \infty} z(t)$ and $\varepsilon = 0.05$. By making $\tilde{\theta}_0$ more negative in (2.97), the system was initialized further and further into a sticking region (This corresponds similarly to increasing k in (2.94)). The results of the settling time T are included in Figure 2-13. Here a decreasing convergence rate for the CRM-adaptive system is observed as $\tilde{\theta}_0$ is made more negative. On the other hand, the IC-adaptive system demonstrates a constant learning rate. Figure 2-13 also includes the settling time T for the exponentially stable system (denoted by ‘EXP-system’) when $\tilde{\Theta}(t) = 0 \forall t$. Here $x(t_1) \neq 0$ such that $\|z(t_1)\| \neq 0$. This additional plot is only included to create a perspective of the convergence rate of the ORM and IC adaptive systems against a roughly equivalent

exponentially stable system.

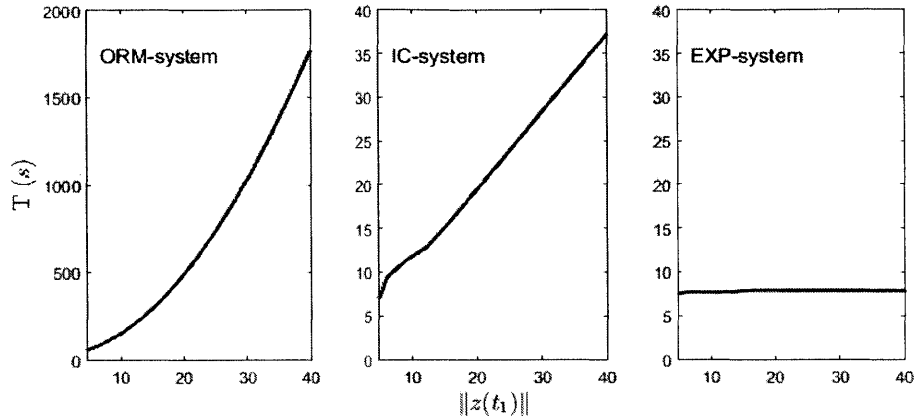


Figure 2-13: Settling time T for various initial conditions of the CRM and IC-adaptive systems

2.4.3 Additional Insight to Sticking in the IC-Adaptive System

The results in Sections 2.3 and 2.4 thus far demonstrate that the IC-adaptive system is less susceptible to sticking when compared to the CRM-adaptive system. Consider again Section 2.1.2: An alternate comparison can be drawn between the two adaptive systems when we note that (2.15) may be written as

$$u(t) = [\Theta_2(t) \dots \Theta_n(t)]x_p(t) + \Theta_1(t) \int_0^t [C_p x_p(\tau) - r(\tau)] d\tau \quad (2.99)$$

where $\Theta(t) = [\Theta_1(t), \Theta_2(t) \dots \Theta_n(t)]$. Let $\Theta_p(t) = [\Theta_2(t) \dots \Theta_n(t)]$ and

$$r_p(t) = q^{*-1} \Theta_1(t) \int_0^t [C_p x_p(\tau) - r(\tau)] d\tau. \quad (2.100)$$

Then (2.99) takes the familiar form

$$u(t) = \Theta_p(t)x_p(t) + q^* r_p(t). \quad (2.101)$$

With this in mind, we compare the IC-adaptive plant differential equation (2.10) and controller (2.101), directly to (2.2) and (2.3) of the CRM-adaptive system. If the order of these

two plants were the same and (A, \mathbf{b}) in (2.2) was equal to (A_p, \mathbf{b}_p) from (2.10), then we expect a very similar result could be drawn from Theorem 2 where the plant states were characterized. This would be the case, but $r_p(t)$ in (2.100) contains a time varying parameter $\Theta_1(t)$ and an integrated error state $e_{yI}(t) = \int_0^t [C_p x_p(\tau) - r(\tau)] d\tau$. Unlike the reference input $r(t)$ in (2.3), $r_p(t)$ introduces an additional degree of freedom that reduces the effects of sticking. It can be seen from (2.29) through (2.32) that the definition of the sticking region \mathcal{S} is largely dependent on the reference input bounds r^* and r_d^* .

2.5 Sticking Analysis with $(A, \lambda \mathbf{b})$ unknown

Thus far in this chapter, we have proved the existence of sticking region in the CRM and IC-adaptive systems for the case when only A in (2.2) and (2.13) was unknown. Consider now the n^{th} order time-invariant plant differential equation is given by

$$\dot{x}(t) = Ax(t) + \lambda \mathbf{b}u(t). \quad (2.102)$$

In this section, we consider the CRM-adaptive system for the case when $(A, \lambda \mathbf{b})$ is unknown. Here it is assumed that the vector \mathbf{b} is known while λ is an unknown constant with a known sign. Once again, only the single input case is considered and it is assumed that the underlying reference input is bounded and smooth. From the numerical analysis in Section 2.4.1, we show that the IC-adaptive system is less susceptible to sticking compared to the CRM-adaptive system. This result could be more intuitively understood from the additional insight provided in Section 2.4.3. Using the same intuitive approach, the effect due to the additional unknown parameter on sticking will be investigated.

In this section we first present the underlying adaptive system when $(A, \lambda \mathbf{b})$ is unknown. The effect of the additional unknown parameter on sticking is then discussed. Finally, simulations are included to verify the result.

2.5.1 The CRM-Adaptive System with $(A, \lambda \mathbf{b})$ Unknown

The n^{th} order time-invariant plant differential equation is given by

$$\dot{x}(t) = Ax(t) + \lambda \mathbf{b}u(t) \quad (2.103)$$

where A is a constant $n \times n$ unknown matrix, \mathbf{b} is a known vector of size n and λ is an unknown scalar with a known sign. A state variable feedback controller is defined by

$$u(t) = \Theta_A(t)x(t) + \Theta_B(t)r(t) \quad (2.104)$$

where $\Theta_A(t)$ and $\Theta_B(t)$ are time varying adaptive parameter updated as

$$\begin{aligned} \dot{\Theta}_A(t) &= -\text{sign}(\lambda) \mathbf{b}^T P e(t) x^T(t) \\ \dot{\Theta}_B(t) &= -\text{sign}(\lambda) \mathbf{b}^T P e(t) r(t) \end{aligned} \quad (2.105)$$

Here $e(t) = x(t) - x_m(t)$ and $x_m(t)$ is the output of a reference model defined by

$$\dot{x}_m(t) = A_m x_m(t) + \mathbf{b}_m r(t) + L e(t) \quad (2.106)$$

where A_m is Hurwitz and L is a constant $n \times n$ feedback matrix which introduces a closed-loop in the reference model. With the standard matching conditions [10]

$$\begin{aligned} A + \lambda \mathbf{b} \Theta_A^* &= A_m \\ \lambda \mathbf{b} \Theta_B^* &= \mathbf{b}_m \end{aligned} \quad (2.107)$$

satisfied, the error differential equation is defined by

$$\dot{e}(t) = [A_m - L]e(t) + \lambda \mathbf{b} \tilde{\Theta}_A(t)x(t) + \lambda \mathbf{b} \tilde{\Theta}_B(t)r(t) \quad (2.108)$$

where $\tilde{\Theta}_A(t) = \Theta_A(t) - \Theta_A^*$ and $\tilde{\Theta}_B(t) = \Theta_B(t) - \Theta_B^*$. If $[A_m - L]$ is Hurwitz, then a symmetric positive definite P exists that solves the well known Lyapunov equation

$$[A_m - L]^T P + P[A_m - L] = -Q_0 \quad (2.109)$$

where Q_0 is a symmetric positive definite matrix. It is well known that the error model in (2.108) and (2.105) can be shown to be globally stable at the origin and that [10]

$$\lim_{t \rightarrow \infty} e(t) = 0. \quad (2.110)$$

2.5.2 Insight to Sticking in the CRM-Adaptive System with $(A, \lambda \mathbf{b})$ Unknown

Using the same approach as presented in Section 2.4.3, we note that the controller in (2.104) may be expressed as

$$u(t) = \Theta_A(t)x(t) + q^* r_B(t) \quad (2.111)$$

where

$$r_B(t) = q^{*-1} \Theta_B(t)r(t). \quad (2.112)$$

With this in mind, we compare the CRM-adaptive plant and controller with $(A, \lambda \mathbf{b})$ unknown in (2.103) and (2.104), directly to (2.2) and (2.3) of the CRM-adaptive system with only (A) unknown. If $(A, \lambda \mathbf{b})$ in (2.103) was equal to (A, \mathbf{b}) form (2.2), then we expect a very similar result could be drawn from Theorem 2 where the plant states were characterized. Once again, this would be the case but $r_B(t)$ in (2.112) contains a time varying parameter $\Theta_B(t)$, which unlike the reference input $r(t)$ in (2.3), introduces an additional degree of freedom that reduces the effects of sticking.

This is a similar result to Section 2.4.3. In order to demonstrate these effects, simulation results are included in the following section.

2.5.3 Simulation Results

Rather than completing an entire sticking analysis for the CRM-adaptive system with $(A, \lambda \mathbf{b})$ unknown, we complete a convergence analysis as done in Section 2.4.2. Simulations were carried out for the CRM-adaptive system with (A) and $(A, \lambda \mathbf{b})$ unknown as defined in Sections 2.1.1 and 2.5.1, respectively. The plant and reference models are defined by

$$A = \begin{bmatrix} 0 & 1 & 0 \\ 0 & 0 & 1 \\ 0 & -4 & -4 \end{bmatrix} \quad \mathbf{b} = \begin{bmatrix} 0 \\ 0 \\ 1 \end{bmatrix} \quad (2.113)$$

$$A_m = \begin{bmatrix} 0 & 1 & 0 \\ 0 & 0 & 1 \\ -1 & -3 & -3 \end{bmatrix} \quad \mathbf{b}_m = \mathbf{b} \quad L = [0_{3 \times 3}]. \quad (2.114)$$

For the CRM-adaptive system with (A) unknown, an adaptive controller as in (2.3) and (2.4) was simulated where P in (2.4) was solved using (2.8) with $Q_0 = I$. For the CRM-adaptive system with $(A, \lambda \mathbf{b})$ unknown, an adaptive controller as in (2.104) and (2.105) was simulated with the same P and $\lambda = 1$. A constant reference input was chosen with $r(t) = 1$ and the system was initialized at $t_1 = 0$ as

$$x(t_1) = 0 \quad x_m(t_1) = 0 \quad \tilde{\Theta}(t_1) = \tilde{\Theta}_A(t_1) = [\tilde{\theta}_0, \tilde{\theta}_0, \tilde{\theta}_0] \quad \tilde{\Theta}_B(t_1) = 0. \quad (2.115)$$

For each simulation, the initial conditions in (2.115) were used for increasingly negative values of $\tilde{\theta}_0$ while recording the settling time T defined as in (2.98) where

$$\begin{aligned} z(t) &= [x(t), x_m(t), \tilde{\Theta}(t)]^T && \text{CRM with only } (A) \text{ unknown} \\ z(t) &= [x(t), x_m(t), \tilde{\Theta}_A(t), \tilde{\Theta}_B(t)]^T && \text{CRM with } (A, \lambda \mathbf{b}) \text{ unknown,} \end{aligned} \quad (2.116)$$

$z^* = \lim_{t \rightarrow \infty} z(t)$ and $\varepsilon = 0.05$. By making $\tilde{\theta}_0$ more negative in (2.97), the system was initialized further and further into a sticking region. The results of the settling time T are included in Figure 2-14. As before, a decreasing convergence rate for the CRM-adaptive

system with only (A) unknown is observed as $\tilde{\theta}_0$ is made more negative. On the other hand, the CRM-adaptive system with $(A, \lambda \mathbf{b})$ unknown demonstrates a constant learning rate similarly to the IC-adaptive system in Figure 2-13. This corresponds to the discussion from Section 2.5.2.

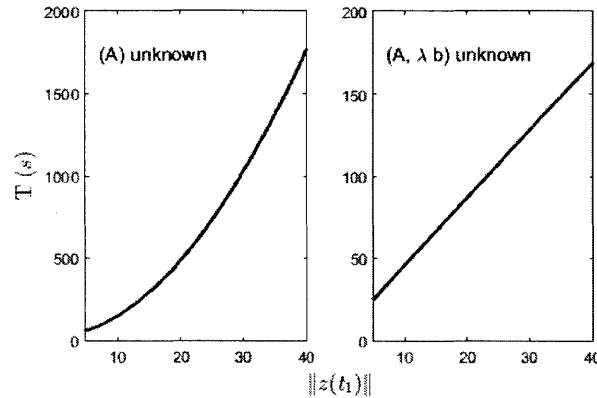


Figure 2-14: Settling time T for various initial conditions of the CRM-adaptive systems with (A) and $(A, \lambda \mathbf{b})$ unknown

2.6 Summary

In this chapter, we have focused on slow convergence properties of errors in a class of adaptive systems that corresponds to adaptive control of linear time-invariant plants with state variables accessible. We prove the existence of a sticking region in the error space where the state errors move with a finite velocity independent of their magnitude. These properties are exhibited by ORM, CRM and IC-adaptive systems. Simulation and numerical studies are included to illustrate the size of this sticking region and its dependence on various system parameters.

Chapter 3

Sticking in Outer-Loop Control

Chapter 2 presents an analytic approach for characterizing sticking regions in adaptive systems. In this chapter, the impact of sticking is investigated for outer-loop controllers that include inner-loop adaptation. An analysis is presented that identifies the existence of a sticking region in the inner-loop and its impact on command following in the outer-loop.

In the design of outer-loop controllers, it is often assumed that the inner-loop states are readily available. The inner control loop is then responsible for tracking command signals generated by the outer-loop. This separates the outer and inner-loop design problems which is advantageous since well-established design methods exist separately [12]. However, if inner-loop adaptation is implemented to account for any uncertainties in the plant model, then it is possible, as argued in Chapter 2, that the overall inner-loop adaptive system can exhibit sticking, and as a result, the outer-loop performance in terms of command tracking can be compromised.

In order to demonstrate these sticking effects in outer-loop control, we focus on a combined inner and outer-loop problem in a flight control application. Here, adaptation is implemented in the inner-loop for control of an aircraft's angle of attack and pitch rate dynamics with uncertainties. This forms the inner-loop dynamics of the system. The outer-loop dynamics consists of the pitch angle and altitude of the aircraft, and is assumed to be known. Two adaptive control solutions are implemented that ensure the aircraft altitude tracks the desired altitude. While the controllers are very similar, they exhibit different behaviors during sticking. Through simulations it is shown that one of these controllers is

not able to access the inner-loop states necessary for effective altitude command tracking during sticking. Thus the importance of accounting for sticking regions in adaptive control is demonstrated.

3.1 Problem Statement

We consider the general outer-loop control problem when the inner-loop dynamics are unknown. Model reference adaptive control may be implemented to account for the uncertainties in the inner-loop. However, following this approach, the system becomes susceptible to inner-loop sticking as presented in Chapter 2. In this section, we present the underlying outer-loop control problem when there are uncertainties in the inner-loop dynamics and propose a control design. With this, the overall problem with regard to the impact of inner-loop sticking on outer-loop control is stated.

3.1.1 The Outer-Loop Control Problem with Unknown Inner-Loop Dynamics

Consider the n_p^{th} order differential equation that describes the unknown inner-loop dynamics given by

$$\dot{x}_p(t) = A_p x_p(t) + \mathbf{b}_p u(t) \quad (3.1)$$

where A_p is a constant unknown $n_p \times n_p$ matrix and \mathbf{b}_p is a known vector of size n_p . Additionally we have the known outer-loop dynamics given by the n_g^{th} order differential equation

$$\begin{aligned} \dot{x}_g(t) &= A_g x_g(t) + B_g x_p(t) \\ y(t) &= C_g x_g(t). \end{aligned} \quad (3.2)$$

It is assumed that the open-loop plant, as shown in Figure 3-1, is controllable with accessible states $x_p(t)$ and $x_g(t)$. Let $y_{cmd}(t)$ be a desired command state which is known and specified. The objective is to design a closed-loop controller $u(t)$ such that the system is

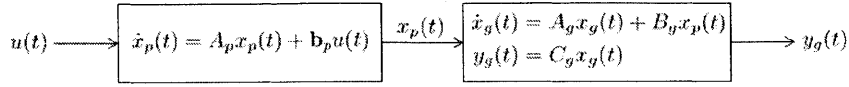


Figure 3-1: Open-loop plant with inner and outer-loop dynamics

stable and the outer-loop state $y_g(t)$ approaches the desired trajectory $y_{gcmd}(t)$, that is

$$\lim_{t \rightarrow \infty} y_g(t) = y_{gcmd}(t). \quad (3.3)$$

In this chapter, the control problem is solved by first designing an open-loop reference model (ORM) where the unknown parameters of the system are estimated. Here the ORM is designed such that it represents the output desired in the plant at every time (i.e. achieves tracking of the trajectory $y_{gcmd}(t)$). Since the dynamics of the reference model may vary from the actual plant, error states are defined. A control architecture similar to that in [14] is then implemented, where additional error state feedback loops are introduced to the ORM, thus forming a closed-loop reference model (CRM). By considering the error dynamics between the actual system and the CRM, an adaptive controller $u(t)$ may be designed to achieve the control objective in (3.3).

The complete control design of $u(t)$ will follow in Section 3.3. In order to present the main idea of this chapter, the following proposition is useful, which is

Proposition 7. *If the uncertainties of the inner-loop dynamics in (3.1) are such that the matching conditions*

$$A_p + \mathbf{b}_p \Theta_p^* = A_{pm} \quad \text{and} \quad \mathbf{b}_p = \mathbf{b}_{pm} \quad (3.4)$$

are satisfied for some Θ_p^ , where A_{pm} and \mathbf{b}_{pm} are known, then there exists an adaptive controller of the form*

$$u(t) = \Theta_p(t)x_p(t) + f_p(t) \quad (3.5)$$

where $\Theta_p(t)$ and $f_p(t)$ are time varying functions with the properties $\Theta_p(t)$, $\dot{\Theta}_p(t)$, $f_p(t)$, $\dot{f}_p(t) \in \mathcal{L}_\infty$ such that the system response satisfies $x_p(t) x_g(t) \in \mathcal{L}_\infty$ and the control objective in (3.3) is realized.

In Proposition 7, the role of the parameters $(A_{pm}, \mathbf{b}_{pm})$ is similar to that of the reference

model discussed in Chapter 2. We will return to the definition of $(A_{pm}, \mathbf{b}_{pm})$ in Section 3.3.

3.1.2 Impact of Inner-Loop Sticking on Outer-Loop Control

Proposition 7 implies that an adaptive controller exists such that the control objective in (3.3) is satisfied. However, by comparing the form of (3.5) to (2.3), we realize the inner-loop may be susceptible to sticking. Thus we begin our approach by completing a sticking analysis as done in Theorem 2 under Proposition 7: Show that there are some initial conditions for which $\tilde{x}_p(t)$ will remain in a set \mathbf{N} while $\tilde{\Theta}_p(t)$ traverses in a set \mathbf{S} over a certain time interval $[t_1, t_2]$. From (3.2), we see that if $x_p(t)$ is subject to the constraint $\tilde{x}_p(t) \in \mathbf{N} \forall t \in [t_1, t_2]$ during sticking, then the ability for $y_g(t)$ to converge quickly towards $y_{gcmd}(t)$ may be prohibited during this time interval.

This is problematic since we have shown in Chapter 2 that sticking may occur for extended periods of time. In this chapter, we are only concerned about the definition of sets \mathbf{S} and \mathbf{N} . Therefore, in this chapter “sticking” will refer to the time interval $[t_1, t_2]$ during which $\tilde{\Theta}(t) \in \mathbf{S}$ and $\tilde{x}(t) \in \mathbf{N}$.

3.2 Analysis of Sticking in Outer-Loop Control

In this section, we complete a sticking analysis as done in Theorems 2 and 6 for the inner-loop of the system as given in (3.1). This is completed using the control solution from Proposition 7 (to be proved in Section 3.3 which addresses the design of an autopilot system for altitude tracking). With this sticking analysis, the impact on outer-loop control will be investigated.

3.2.1 Inner-Loop Sticking

Suppose that the matching condition is satisfied for a suitably chosen $(A_{pm}, \mathbf{b}_{pm})$ and that a control input as in (3.5) exists. We can then express the plant differential equation in (3.1)

as

$$\dot{x}_p(t) = [A_{pm} + \mathbf{b}_p \tilde{\Theta}_p(t)]x_p(t) + \mathbf{b}_p f_p(t) \quad (3.6)$$

where $\tilde{\Theta}_p(t) = \Theta_p(t) - \Theta_p^*$. Following the same approach as presented in Section 2.2.1, we consider an arbitrary point Θ_{p0} , and a fictitious trajectory $\hat{x}_p(t)$ and the deviation $\tilde{x}_p(t)$ of $x_p(t)$ from $\hat{x}_p(t)$. That is, we define

$$\tilde{\Theta}_p(t) = \Theta_{p0} + \delta \tilde{\Theta}_p(t) \quad (3.7)$$

$$\hat{x}_p(t) = -[A_{pm} + \mathbf{b}_p \Theta_{p0}]^{-1} \mathbf{b}_p f_p(t) \quad (3.8)$$

$$\tilde{x}_p(t) = x_p(t) - \hat{x}_p(t). \quad (3.9)$$

Using equations (3.6) through (3.9), a differential equation for the state $\tilde{x}_p(t)$ may be expressed as

$$\dot{\tilde{x}}_p(t) = \hat{A}_p(\tilde{\Theta}_p(t))\tilde{x}_p(t) + \mathbf{w}_p(t) \quad (3.10)$$

where $\hat{A}_p(\tilde{\Theta}_p(t)) = [A_{pm} + \mathbf{b}_p \tilde{\Theta}_p(t)]$ and $\mathbf{w}_p(t) = \mathbf{b}_p \delta \tilde{\Theta}_p(t) \hat{x}_p(t) - \dot{\hat{x}}_p(t)$. We notice that (3.10) is identical to (2.27), thus we may use Theorems 2 and 6 as given in Chapter 2. For convenience, these theorems are included in Table 3.1 with the newly defined variables. We note that the only major difference is that the reference input from Chapter 2, has been replaced by the bounded and smooth time varying function $f_p(t)$ that is yet to be defined.

3.2.2 Outer-Loop Sticking

The impact of inner-loop sticking on outer-loop control will be demonstrated in Section 3.3. It will be shown that there exists transfer function $G(s)$ such that

$$x_g(s) - x_{gORM}(s) = G(s)e_x(s). \quad (3.11)$$

Here $e_x(t)$ is an error state of the system measured from the CRM and $x_{gORM}(s)$ is the outer-loop state of the ORM. Precise definitions will follow in Section 3.3. At this stage, it is only important to note that as per the ORM design, $x_{gORM}(t)$ represents the output desired in the outer-loop of the plant.

Table 3.1: Definitions for the inner-loop sticking analysis

Definition	Equivalent Eqn. from Chapter 2	Description / Notes
$\tilde{\Theta}_p(t) = \Theta_{p0} + \delta\tilde{\Theta}_p(t)$	2.23	
$\hat{x}_p(t) = -[A_{pm} + \mathbf{b}_p\Theta_{p0}]^{-1}\mathbf{b}_pf_p(t)$	2.24	Fictitious trajectory
$\tilde{x}_p(t) = x_p(t) - \hat{x}_p(t)$	2.25	Deviation of $x_p(t)$ from $\hat{x}_p(t)$
$\hat{A}_{p0} = A_{pm} + \mathbf{b}_p\Theta_{p0}$	2.63	\hat{A}_{p0} must be Hurwitz for Theorem 6 to apply
$\hat{A}_{p0}^T\bar{Y} + \bar{Y}\hat{A}_{p0} = -I$	2.61	
$Y = (1 + \gamma^2)\bar{Y}$	2.62	Here γ^2 is an arbitrary positive constant
Define f^* such that $ f_p(t) \leq f^* \forall t$		
Define f_d^* such that $ \dot{f}_p(t) \leq f_d^* \forall t$		
$\beta \geq \frac{\ (A_{pm} + \mathbf{b}_p\Theta_{p0})^{-1}\mathbf{b}_p\ \times (\ Y\mathbf{b}_p\ ^{1-\alpha}f^* + \ Y\ f_d^*)}{\ Y\mathbf{b}_p\ ^\alpha}$	2.32	Here $0 \leq \alpha \leq 1$
$\mathbf{S} : \left\{ \tilde{\Theta}_p \in \mathbb{R}^{n_p} \mid [\hat{A}^T(\tilde{\Theta}_p)Y + Y\hat{A}(\tilde{\Theta}_p) + I] < 0 \cap \ \tilde{\Theta}_p - \Theta_{p0}\ \leq \ Y\mathbf{b}_p\ ^{-\alpha} \right\}$	2.29	Here $\hat{A}(\tilde{\Theta}_p(t)) = [A_{pm} + \mathbf{b}_p\tilde{\Theta}_p(t)]$
$\mathbf{N} : \left\{ \tilde{x}_p \in \mathbb{R}^{n_p} \mid \tilde{x}_p^T Y \tilde{x}_p \leq 4\lambda_{\max}(Y)\beta^2 \right\}$	2.31	

Theorems

Theorem 2. If (i) $\tilde{\Theta}_p(t) \in \mathbf{S} \forall t \in [t_1, t_2]$ where $t_2 > t_1$, and (ii) $\tilde{x}_p(t_1) \in \mathbf{N}$, then

$$\tilde{x}_p(t) \in \mathbf{N} \forall t \in [t_1, t_2].$$

Theorem 6. Let

$$\hat{A}_{p0} = A_{pm} + \mathbf{b}_p\Theta_{p0}$$

be Hurwitz. Then \mathbf{S} exists and may be defined as

$$\mathbf{S} : \left\{ \tilde{\Theta}_p \in \mathbb{R}^{n_p} \mid -\delta\Theta_p^* \leq \tilde{\Theta}_p - \Theta_{p0} \leq \delta\Theta_p^* \right\}$$

where

$$\delta\Theta_p^* = [\delta\theta_p^*, \delta\theta_p^* \dots \delta\theta_p^*]$$

with

$$0 < \delta\theta_p^* < \min \left\{ \frac{\gamma^2}{2n_p\|Y\mathbf{b}_p\|_{\max}}, \frac{1}{n_p\|Y\mathbf{b}_p\|^\alpha} \right\}.$$

Through Proposition 7, we may use the inner-loop sticking analysis as presented in Table 3.1. If sticking imposes the constraint $\tilde{x}_p(t) \in \mathbf{N} \forall t \in [t_1, t_2]$ such that $\|e_x(t)\| > 0 \forall t \in T$ where $T \subset [t_1, t_2]$, then $x_g(t)$ will converge slowly to $x_{gORM}(t)$. From (3.11), this is clear since ideally we require $e_x(t) = 0 \forall t$. Of course, $G(s)$ must be more closely examined to make this conclusion as will be done in the simulation study at the end of this chapter.

From the design of the adaptive controller in Proposition 7, we know that $y_g(t)$ will approach $y_{gcmd}(t)$ eventually. However, we do not know how quickly $y_g(t)$ will approach $y_{gcmd}(t)$. The above approach will help us qualify this convergence rate in the outer-loop.

A more intuitive understanding may be gained if (3.2) is considered in isolation: It is a well know result that stability and controllability can not be guaranteed for on open-loop unstable system, such as perhaps (3.2), if the input is constrained [7]. Sticking constrains the “input” $x_p(t)$ for a finite duration of time, therefore, the system might not behave like a controllable or stable system during this finite time. It is only once the system leaves the sticking region that the designed stability, controllability and tracking is observed.

3.3 Outer-Loop Altitude Control with Inner-Loop Adaptation

In this section, we demonstrate the impact of inner-loop sticking on outer-loop control with a practical application of altitude control for an aircraft. Here, adaptation is implemented in the inner-loop for control of an aircraft’s angle of attack $\alpha(t)$ and pitch rate $q(t)$ dynamics with uncertainties. This is called the short period dynamics of the aircraft and forms the inner-loop dynamics of the plant which is represented by (3.1), therefore $x_p(t) = [\alpha(t), q(t)]^T$.

The outer-loop dynamics consist of the pitch angle $\theta(t)$ and altitude $h(t)$ of the aircraft which is represented by (3.2) such that $x_g(t) = [\theta(t), h(t)]^T$. The control system’s objective is to track a desired altitude command signal $h_{cmd}(t)$, therefore the objective in (3.3)

becomes

$$\lim_{t \rightarrow \infty} h(t) = h_{cmd}(t). \quad (3.12)$$

The controller $u(t)$ will be as defined in Proposition 7, thus we know that the state $x_p(t)$ may be susceptible to sticking from Theorems 2 and 6 in Table 3.1 which will impact the outer-loop control as discussed in Section 3.2.

This section is presented as follows: First the underlying control problem with model uncertainties is formulated from which an ORM is designed. By implementing a closed-loop structure as done in [14], a CRM is defined from the ORM. With this control structure, two adaptive controllers are designed which prove Proposition 7. Finally, the simulations are included to demonstrate the impact of inner-loop sticking on outer-loop control.

3.3.1 Control Problem Formulation

Before a controller can be designed, it is required to model the aircraft for the necessary longitudinal dynamics. In this section, these dynamics will be decoupled to form the inner and outer-loop dynamics which will form the model as described in (3.1) and (3.2), respectively. The numerical values that define this model will also be included for the simulation that follows at the end of this chapter. Finally, the model uncertainties as represented by (3.4) will be discussed for the aircraft.

Longitudinal and Guidance Dynamics

The longitudinal dynamics of an aircraft describes the forward, vertical and pitching motion of the vehicle. By linearizing the dynamics about a trim condition, the following model which describes the longitudinal flight dynamics is obtained: [9] [14]:

$$\begin{bmatrix} \dot{V}_T \\ \dot{\alpha} \\ \dot{q} \\ \dot{\theta} \\ \dot{h} \end{bmatrix} = \begin{bmatrix} X_V & X_\alpha & 0 & -g \cos \gamma_0 & X_h \\ \frac{Z_V}{V_0} & \frac{Z_\alpha}{V_0} & 1 + \frac{Z_q}{V_0} & -\frac{g \sin \gamma_0}{V_0} & 0 \\ M_V & M_\alpha & M_q & 0 & 0 \\ 0 & 0 & 1 & 0 & 0 \\ \sin \gamma_0 & -V_0 \cos \gamma_0 & 0 & V_0 \cos \gamma_0 & 0 \end{bmatrix} \begin{bmatrix} V_T \\ \alpha \\ q \\ \theta \\ h \end{bmatrix} + \begin{bmatrix} X_{\delta_{th}} \cos \alpha_0 & X_{\delta_e} \\ -X_{\delta_{th}} \sin \alpha_0 & \frac{Z_{\delta_e}}{V_0} \\ M_{\delta_{th}} & M_{\delta_e} \\ 0 & 0 \\ 0 & 0 \end{bmatrix} \begin{bmatrix} \delta_{th} \\ \delta_e \end{bmatrix}. \quad (3.13)$$

Here it is assumed that the thrust line is aligned with the forward axis of the aircraft. The states are given by the forward velocity $V_T(t)$, the angle of attack $\alpha(t)$, the pitch rate $q(t)$, the pitch angle $\theta(t)$ and altitude $h(t)$. Figure 3-2 shows some of these states and their relation to the flight path angle $\gamma(t) = \theta(t) - \alpha(t)$. Additionally, V_0 is the trimmed airspeed,

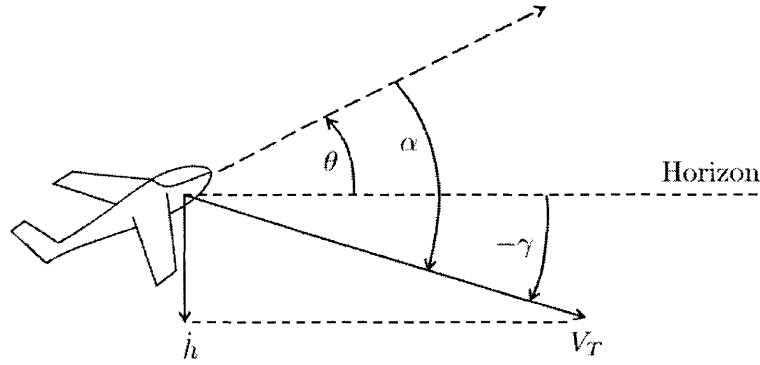


Figure 3-2: Longitudinal flight angle relations [9]

α_0 is the trimmed angle of attack, $\gamma_0 = \theta_0 - \alpha_0$ is the trimmed flight path angle and θ_0 is the trimmed pitch angle. Finally, $\delta_{th}(t)$ and $\delta_e(t)$ denote the thrust and elevator inputs, respectively, relative to the trim condition. The matrix components of (3.13) represent constant stability and control derivatives of the aircraft forces and moments.

For some flight vehicles, a strong decoupling follows from a modal analysis of (3.13) between the velocity dynamics and remaining longitudinal dynamics [9] as is the case considered in this chapter. The decoupled velocity dynamics are then given by

$$\dot{V}_T(t) = X_V V_T(t) + X_{\delta_{th}} \cos \alpha_0 \delta_{th}(t). \quad (3.14)$$

For simplicity, we assume $\delta_{th}(t)$ is controlled such that $V_T(t) = V_0$. Furthermore, we assume a trim condition such that the $-\frac{g \sin \gamma_0}{V_0}$ term in (3.13) is negligible. Thus, the *short period dynamics* of the aircraft are extracted as

$$\begin{bmatrix} \dot{\alpha} \\ \dot{q} \end{bmatrix} = \begin{bmatrix} \frac{Z_\alpha}{V_0} & 1 + \frac{Z_q}{V_0} \\ M_\alpha & M_q \end{bmatrix} \begin{bmatrix} \alpha \\ q \end{bmatrix} + \begin{bmatrix} \frac{Z_{\delta_e}}{V_0} \\ M_{\delta_e} \end{bmatrix} \delta_e. \quad (3.15)$$

Let $x_p(t) = [\alpha(t), q(t)]^T$ and $u(t) = \delta_e(t)$, then (3.15) may be written as

$$\dot{x}_p(t) = A_p x_p(t) + \mathbf{b}_p u(t) \quad (3.16)$$

which forms the inner-loop dynamics of the control problem as given in (3.1). The remaining dynamics are given by

$$\begin{bmatrix} \dot{\theta} \\ \dot{h} \end{bmatrix} = \begin{bmatrix} 0 & 0 \\ V_0 \cos \gamma_0 & 0 \end{bmatrix} \begin{bmatrix} \theta \\ h \end{bmatrix} + \begin{bmatrix} 0 & 1 \\ -V_0 \cos \gamma_0 & 0 \end{bmatrix} \begin{bmatrix} \alpha \\ q \end{bmatrix}. \quad (3.17)$$

Let $x_g(t) = [\theta(t), h(t)]^T$, then from (3.17) we obtain

$$\begin{aligned} \dot{x}_g(t) &= A_g x_g(t) + B_g x_p(t) \\ h(t) &= C_g x_g(t) \end{aligned} \quad (3.18)$$

where $C_g = [0, 1]$ which forms the outer-loop dynamics given in (3.2). The simulations in this chapter will be carried out on an aircraft with a flight condition of Mach 0.3, 5,000 *ft* altitude, trim angle-of-attack of $\alpha_0 = 5^\circ$. The stability and control derivatives with trim conditions are included in Table 3.2 [9]. This fully defines the unknown inner-loop dynamics and known outer-loop dynamics in (3.16) and (3.18), respectively.

Representation of Uncertainties and the Matching Condition

An adaptive controller will be designed to account for any uncertainties of the stability and control derivatives in the inner-loop model given by (3.16). We assume the uncertainties are represented by the matching conditions

$$A_p + \mathbf{b}_p \Theta_p^* = A_{pm} \quad \text{and} \quad \mathbf{b}_p = \mathbf{b}_{pm}. \quad (3.19)$$

where A_{pm} and \mathbf{b}_{pm} are known, thus satisfying (3.4) in Proposition 7. Following the definition of (A_p, \mathbf{b}_p) in (3.15), we see that if V_0 is much greater in magnitude than Z_α , Z_q and Z_{δ_e} , then only control derivative M_{δ_e} must be known. This is true since for some uncertainties in Z_α , Z_q and Z_{δ_e} , the matching condition can be approximately satisfied. The

uncertainties and estimation of parameters are included in Table 3.2. With this we define $(A_{pm}, \mathbf{b}_{pm})$ as the estimate of (A_p, \mathbf{b}_p) such that

$$A_{pm} = \begin{bmatrix} \frac{Z_{\alpha m}}{V_0} & 1 + \frac{Z_{qm}}{V_0} \\ M_{\alpha m} & M_{qm} \end{bmatrix} \quad \text{and} \quad \mathbf{b}_{pm} = \begin{bmatrix} \frac{Z_{\delta_e m}}{V_0} \\ M_{\delta_e} \end{bmatrix}. \quad (3.20)$$

In designing the ORM, $(A_{pm}, \mathbf{b}_{pm})$ will be used to describe the reference model inner-loop dynamics.

Table 3.2: Stability and control derivatives with uncertainties

Inner-loop (A_p, \mathbf{b}_p) and outer-loop (A_g, B_g) model parameters in (3.15) and (3.17)	Estimated parameters	Uncertainty
$Z_\alpha = -1.0527 (1/s)$	$Z_{\alpha m} = -1.5$	< 50%
$Z_q = 0 (1/s)$	$Z_{qm} = 0 (1/s)$	Known
$Z_{\delta_e} = -0.0343 (1/s)$	$Z_{\delta_e m} = 0(1/s)$	100%
$M_\alpha = -2.3294 (1/s^2)$	$M_{\alpha m} = -6 (1/s^2)$	< 200%
$M_q = -1.0334 (1/s^2)$	$M_{qm} = -2 (1/s^2)$	< 100%
$M_{\delta_e} = -1.1684 (1/s^2)$	$M_{\delta_e m} = M_{\delta_e} (1/s^2)$	Known
$V_0 = 329.13 (ft/s)$	$V_{0m} = V_0$	Known
$\gamma_0 = 0^\circ$	$\gamma_{0m} = \gamma_0$	Known

3.3.2 Open-Loop Reference Model Design

An ORM must be designed to represent the output desired in the plant at every time, from which a CRM can be defined by implementing a closed-loop architecture similar to that in [14]. With this control structure, the adaptive controllers may be designed. In the ORM, an inner-loop is designed around the estimated short period dynamics, which will implement integral action for command tracking of the signal $\alpha_{m_{cmd}}(t)$ with the angle of attack. A forward-loop controller will be responsible for generating this command signal in a way such that the ORM represents a desired output. Finally, these dynamics will be combined

with the outer-loop dynamics to form the ORM. The ORM block diagram is shown in Figure 3-3, of which each component will be designed in this section.

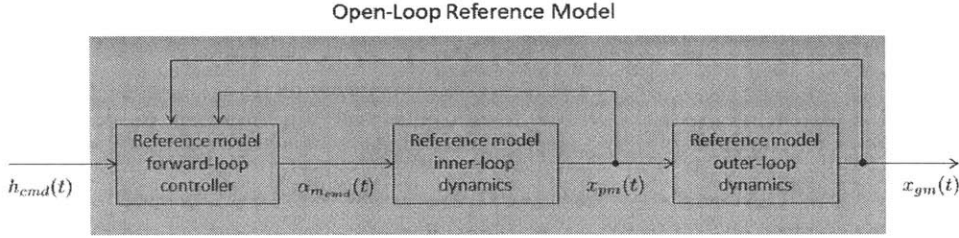


Figure 3-3: Open-loop reference model block diagram

Reference Model Inner and Outer-loop Dynamics with Integral Action for Angle of Attack Tracking

We define the reference model inner-loop dynamics as

$$\dot{x}_{pm}(t) = A_{pm}x_{pm}(t) + \mathbf{b}_{pm}u_m(t) \quad (3.21)$$

where $(A_{pm}, \mathbf{b}_{pm})$ is defined in (3.20) and follows the matching condition in (3.19). The states $x_{pm}(t) = [\alpha_m(t), q_m(t)]^T$ represent the reference model angle of attack and pitch rate. The reference model outer-loop dynamics are given by

$$\begin{aligned} \dot{x}_{gm}(t) &= A_g x_{gm}(t) + B_g x_{pm}(t) \\ h_m(t) &= C_g x_{gm}(t) \end{aligned} \quad (3.22)$$

where the states $x_{gm}(t) = [\theta_m(t), h_m(t)]^T$ represent the reference model pitch angle and altitude and $C_g = [0, 1]$. Also, A_g and B_g are as defined in (3.17) and (3.18). In order to introduce command tracking, the additional integral error state is defined by

$$\dot{e}_{yIm}(t) = C_p x_{pm}(t) - \alpha_{m_{cmd}}(t) \quad (3.23)$$

where $C_p = [1, 0]$ such that $C_p x_{pm}(t) = \alpha_m(t)$. As done in Section (2.1.2), an augmented system is created in order to include the state $e_{yIm}(t)$ as follows:

$$\begin{bmatrix} \dot{e}_{yIm} \\ \dot{x}_{pm} \end{bmatrix} = \begin{bmatrix} 0 & C_p \\ 0_{n_p \times 1} & A_{pm} \end{bmatrix} \begin{bmatrix} e_{yIm} \\ x_{pm} \end{bmatrix} + \begin{bmatrix} 0 \\ \mathbf{b}_{pm} \end{bmatrix} u_m + \begin{bmatrix} -1 \\ 0_{n_p \times 1} \end{bmatrix} \alpha_{m_{cmd}}(t). \quad (3.24)$$

Since state variables $[e_{yIm}(t), x_{pm}^T(t)]^T$ are accessible, we introduce feedback with

$$u_m(t) = -K[e_{yIm}(t), x_{pm}^T(t)]^T \quad (3.25)$$

to obtain

$$\begin{bmatrix} \dot{e}_{yIm} \\ \dot{x}_{pm} \end{bmatrix} = \left(\begin{bmatrix} 0 & C_p \\ 0_{n_p \times 1} & A_{pm} \end{bmatrix} - \begin{bmatrix} 0 \\ \mathbf{b}_{pm} \end{bmatrix} K \right) \begin{bmatrix} e_{yIm} \\ x_{pm} \end{bmatrix} + \begin{bmatrix} -1 \\ 0_{n_p \times 1} \end{bmatrix} \alpha_{m_{cmd}}(t). \quad (3.26)$$

We may represent (3.26) more compactly as

$$\dot{x}_m(t) = A_m x_m(t) + \mathbf{b}_m \alpha_{m_{cmd}}(t) \quad (3.27)$$

where $x_m(t) = [e_{yIm}(t), x_{pm}(t)^T]^T$. The feedback K may be chosen with LQR or by other means such that A_m is Hurwitz. In the next section, we design a forward-loop controller to generate the command signal $\alpha_{m_{cmd}}(t)$.

Forward-Loop Controller Design

We must now design a forward-loop controller which will specify the command signal $\alpha_{m_{cmd}}(t)$ in (3.27). In order to do this, we consider a known guidance method for altitude control in an aircraft. Many guidance algorithms specify acceleration command signals for the inner-loop to track. This is a natural selection since limitations of the vehicle may easily be related to acceleration limits (maximum g-forces) [4]. Additionally, the acceleration of a vehicle is usually a state that may be derived from the inner-loop, thus command signal tracking techniques may be implemented directly. We begin with a guidance method that

follows a pure pursuit based approach adapted from [1], [3], [11]:

$$A_{z_{cmd}}(t) = -k_g \frac{V_0^2}{L_1} \sin \eta(t) \quad \text{with } k_g > 0. \quad (3.28)$$

Here a reference point is created on a precomputed desired altitude trajectory $h_{cmd}(t)$ that lies at a distance L_1 forward of the aircraft. Based on the aircraft's current flight path angle and velocity, an acceleration command $A_{z_{cmd}}(t)$ is specified that will advance the vehicle towards the reference point. Figure 3-4 more clearly illustrates the method. It should be

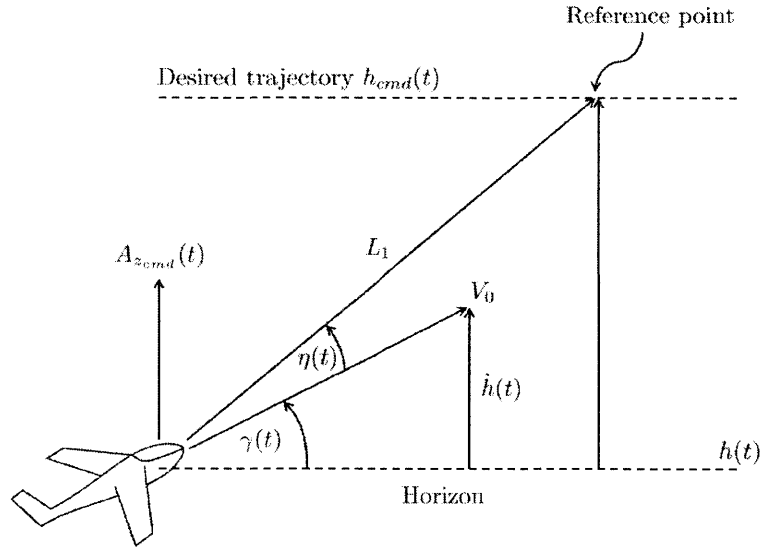


Figure 3-4: Pursuit based guidance algorithm [3]

noted that the convention is to measure the vertical acceleration positive in the downward direction, while the altitude is measured positive in the upward direction. At this point we note that the vertical acceleration is not an available inner-loop state. Therefore we use

$$\begin{aligned} A_z(t) &= -\ddot{h}(t) = -V_0 \cos \gamma_0 (\dot{\theta}(t) - \dot{\alpha}(t)) = V_0 \cos \gamma_0 (\dot{\alpha}(t) - q(t)) \\ &= \cos \gamma_0 (Z_\alpha \alpha(t) + Z_q q(t) + Z_{\delta_e} u(t)) \end{aligned} \quad (3.29)$$

From the parameters in Table 3.2, we approximate this relation with

$$A_z(t) \approx Z_\alpha \alpha(t) \quad (3.30)$$

which implies that $A_{z_{cmd}}(t) \approx Z_\alpha \alpha_{cmd}(t)$. With this and $k_g = -2Z_\alpha > 0$ in (3.28), the guidance method becomes

$$\alpha_{cmd}(t) = 2 \frac{V_0^2}{L_1} \sin \eta(t). \quad (3.31)$$

By assuming $\gamma(t)$ and $\eta(t)$ remain small and $L_1 \gg |h_{cmd}(t) - h(t)|$, the guidance method in (3.31) is linearized as

$$\alpha_{cmd}(t) = \frac{2}{L_1} \left[F_p x_p(t) + F_g x_g(t) + F_{cmd} h_{cmd}(t) \right] \quad (3.32)$$

where

$$F_p = \begin{bmatrix} V_0^2 & 0 \end{bmatrix} \quad F_g = \begin{bmatrix} -V_0^2 & -\frac{V_0^2}{L_1} \end{bmatrix} \quad F_{cmd} = \begin{bmatrix} \frac{V_0^2}{L_1} \end{bmatrix}, \quad (3.33)$$

thus forming the forward-loop controller. Of course, for the ORM we implement the same methodology, but computed from the reference model states such that

$$\alpha_{m_{cmd}}(t) = \frac{2}{L_1} \left[F_p x_{pm}(t) + F_g x_{gm}(t) + F_{cmd} h_{cmd}(t) \right] \quad (3.34)$$

which forms the reference model forward-loop controller.

Completing the ORM Design

The reference dynamics from (3.22) and (3.27) are combined with the forward-loop controller in (3.34) to produce the ORM given by

$$\begin{bmatrix} \dot{x}_m \\ \dot{x}_{gm} \end{bmatrix} = \begin{bmatrix} A_m + [0_{(n_p+1) \times 1}, \mathbf{b}_m F_p] & \mathbf{b}_m F_g \\ [0_{n_g \times 1}, B_g] & A_g \end{bmatrix} \begin{bmatrix} x_m \\ x_{gm} \end{bmatrix} + \begin{bmatrix} \mathbf{b}_m F_{cmd} \\ 0_{n_g \times 1} \end{bmatrix} h_{cmd}(t). \quad (3.35)$$

Once again, the reference model parameters are given in Table 3.2. We let $K = [-1, 0, 0]$ and $L_1 = 12,000 \text{ ft}$ such that the ORM in (3.35) is stable. The pole-zero map and step response of the transfer function $\frac{h_m(s)}{h_{cmd}(s)}$ is shown in Figure 3-5 which confirms that the ORM represents a desired output. This defines the ORM response $x_{gORM}(s)$ in (3.11).

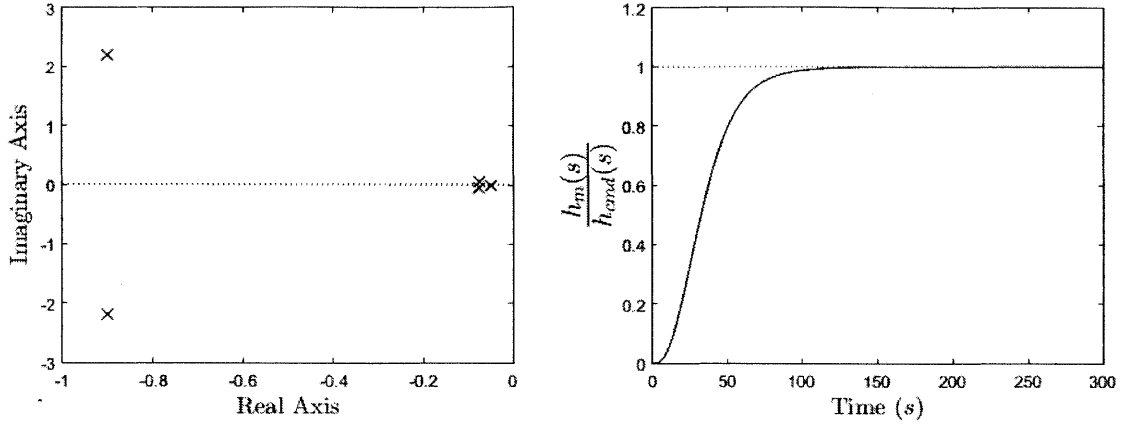


Figure 3-5: Open-loop reference model pole-zero map and step response

3.3.3 Adaptive Control Design

Section 3.3.2 describes the design procedure of the ORM. In this section, additional error state feedback loops will be introduced to the ORM to form the CRM. With this closed-loop architecture, we can introduce adaptive control through the design of the elevator input $u(t)$ in (3.16) and prove Proposition 7.

Error Dynamics and the Closed-Loop Reference Model

The inner-loop dynamics are given by (3.16). As done in Section 3.3.2, an additional integral error state is defined in order to introduce command tracking of the command signal $\alpha_{cmd}(t)$ with the angle of attack given by

$$\dot{e}_{yl}(t) = C_p x_p(t) - \alpha_{cmd}(t) \quad (3.36)$$

where C_p and $\alpha_{cmd}(t)$ were previously defined in (3.23) and (3.32), respectively. Again, an augmented system is created in order to include the state e_{yl} as follows:

$$\begin{bmatrix} \dot{e}_{yl} \\ \dot{x}_p \end{bmatrix} = \begin{bmatrix} 0 & C_p \\ 0_{n_p \times 1} & A_p \end{bmatrix} \begin{bmatrix} e_{yl} \\ x_p \end{bmatrix} + \begin{bmatrix} 0 \\ \mathbf{b}_p \end{bmatrix} u + \begin{bmatrix} -1 \\ 0_{n_p \times 1} \end{bmatrix} \alpha_{cmd}. \quad (3.37)$$

We represent (3.37) as

$$\dot{x}(t) = Ax(t) + \mathbf{b}u(t) + \mathbf{b}_m\alpha_{cmd}(t) \quad (3.38)$$

where $x(t) = [e_{yl}(t), x_p^T(t)]^T$. The inner-loop error is defined through the inner-loop dynamics in (3.38) and the reference model inner-loop dynamics in (3.27) with

$$e_x(t) = x(t) - x_m(t) \quad (3.39)$$

The outer-loop error is defined through the outer-loop dynamics in (3.18) and the reference model outer-loop dynamics in (3.22) with

$$e_g(t) = x_g(t) - x_{gm}(t). \quad (3.40)$$

From (3.39), (3.40) and the ORM in (3.35), we select the CRM as

$$\begin{aligned} \begin{bmatrix} \dot{x}_m \\ \dot{x}_{gm} \end{bmatrix} &= \begin{bmatrix} A_m + [0_{(n_p+1) \times 1}, \mathbf{b}_m F_p] & \mathbf{b}_m F_g \\ [0_{n_g \times 1}, B_g] & A_g \end{bmatrix} \begin{bmatrix} x_m \\ x_{gm} \end{bmatrix} \\ &+ \begin{bmatrix} \mathbf{b}_m F_{cmd} \\ 0_{n_g \times 1} \end{bmatrix} h_{cmd} + \begin{bmatrix} L_x & \mathbf{b}_m F_g \\ [0_{n_g \times 1}, B_g] & L_g \end{bmatrix} \begin{bmatrix} e_x \\ e_g \end{bmatrix}. \end{aligned} \quad (3.41)$$

By introducing the error-state feedback in (3.41), we create a CRM as described in Section 2.1.1 which has been shown to provide improved transient properties over classical reference models [5][6]. Additionally, the feedback matrices $[0_{n_g \times 1}, B_g]$, $\mathbf{b}_m F_g$ allow us to decouple the error dynamics of $e_x(t)$ and $e_g(t)$ and achieve the desired control objective with stability as will be shown in the next section. This method was introduced by [14].

From (3.38), (3.39) and (3.41), the inner-loop error dynamics are given by

$$\begin{aligned} \dot{e}_x(t) &= Ax(t) - A_m x_m(t) + \mathbf{b}u(t) + \mathbf{b}_m(\alpha_{cmd}(t) - \alpha_{m_{cmd}}(t)) - L_x e_x(t) - \mathbf{b}_m F_g e_g(t) \\ &= Ax(t) - A_m x_m(t) + \mathbf{b}u(t) + \mathbf{b}_m[0, F_p]e_x(t) - L_x e_x(t). \end{aligned} \quad (3.42)$$

However, through the matching condition in (3.19) and the definitions of A and A_m in (3.37)

and (3.26), respectively, we have

$$\begin{aligned}
 A &= \begin{bmatrix} 0 & C_p \\ 0_{n_p \times 1} & A_{pm} \end{bmatrix} - \begin{bmatrix} 0 & 0_{1 \times n_p} \\ 0_{n_p \times 1} & \mathbf{b}_p \Theta_p^* \end{bmatrix} - \begin{bmatrix} 0 \\ \mathbf{b}_{pm} \end{bmatrix} K + \begin{bmatrix} 0 \\ \mathbf{b}_{pm} \end{bmatrix} K \\
 &= A_m + \begin{bmatrix} 0 \\ \mathbf{b}_p \end{bmatrix} K - \begin{bmatrix} 0 & 0_{1 \times n_p} \\ 0_{n_p \times 1} & \mathbf{b}_p \Theta_p^* \end{bmatrix} \\
 &= A_m - \mathbf{b} [[0, \Theta_p^*] - K].
 \end{aligned} \tag{3.43}$$

Substituting (3.43) in (3.42) gives

$$\dot{e}_x(t) = [A_m - L_x + \mathbf{b}_m [0, F_p]] e_x(t) + \mathbf{b} (u(t) - [[0, \Theta_p^*] - K] x(t)). \tag{3.44}$$

From (3.18), (3.40) and (3.41) the outer-loop error dynamics are given by

$$\dot{e}_g(t) = [A_g - L_g] e_g(t). \tag{3.45}$$

The control architecture with error state feedback loops is shown in Figure 3-6.

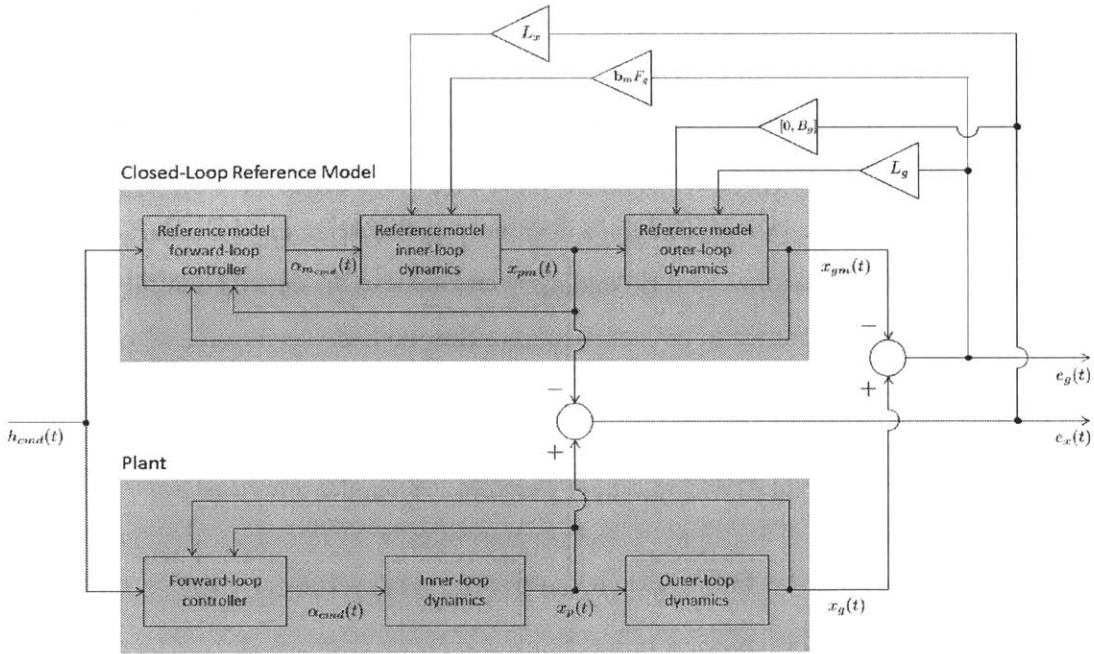


Figure 3-6: Control architecture with error state feedback loops

Adaptive Control of $u(t)$

The objective of the adaptive system is to design the control input $u(t)$ such that

$$\begin{aligned}\lim_{t \rightarrow \infty} e_x(t) &= 0 \\ \lim_{t \rightarrow \infty} e_g(t) &= 0.\end{aligned}\tag{3.46}$$

This will allow the autopilot to achieve the desired output of the ORM. This can be accomplished in two methods, both of which are outlined in the theorems to follow. Here the control design in Theorem 8 corresponds to the IC-adaptive controller as done in [14]. On the other hand, Theorem 9 implements a controller with one less adaptive parameter compared to the control design in Theorem 8. This is done by using the fact that \mathbf{b} in (3.38) is known, which results in a less complex controller.

Theorem 8. *Let*

$$\begin{aligned}u(t) &= \Theta_p(t)x_p(t) + \Theta_{yI}(t)e_{yI}(t) \\ &= [\Theta_{yI}(t), \Theta_p(t)]x(t)\end{aligned}\tag{3.47}$$

where $\Theta_p(t)$ and $\Theta_{yI}(t)$ are updated as

$$[\dot{\Theta}_{yI}(t), \dot{\Theta}_p(t)] = -\mathbf{b}^T P_x e_x(t) x^T(t).\tag{3.48}$$

If (i) L_x is chosen such that $[A_m - L_x + \mathbf{b}_m[0, F_p]]$ is Hurwitz and P_x is defined by

$$[A_m - L_x + \mathbf{b}_m[0, F_p]]^T P_x + P_x [A_m - L_x + \mathbf{b}_m[0, F_p]] = -Q_x\tag{3.49}$$

where Q_x is symmetric positive definite and (ii) L_g is chosen such that $[A_g - L_g]$ is Hurwitz, then the system is globally stable and $\lim_{t \rightarrow \infty} e_x(t) = 0$ and $\lim_{t \rightarrow \infty} e_g(t) = 0$.

Proof. With the adaptive control law in (3.47), the error dynamics in (3.44) becomes

$$\dot{e}_x(t) = [A_m - L_x + \mathbf{b}_m[0, F_p]]e_x(t) + \mathbf{b}\tilde{\Theta}(t)x(t)\tag{3.50}$$

where

$$\tilde{\Theta}(t) = [\Theta_{yI}(t), \Theta_p(t)] - [[0, \Theta_p^*] - K]. \quad (3.51)$$

We define the radially unbounded Lyapunov function candidate

$$V(t) = e_g^T(t)P_g e_g(t) + e_x^T(t)P_x e_x(t) + Tr[\tilde{\Theta}^T(t)\tilde{\Theta}(t)]. \quad (3.52)$$

Here P_g is the solution to the Lyapunov equation

$$[A_g - L_g]^T P_g + P_g [A_g - L_g] = -Q_g \quad (3.53)$$

where Q_g is symmetric positive definite. It follows that P_x and P_g are positive definite from condition (i) and (ii) of Theorem 8. From (3.45), (3.48), (3.53) and condition (i) of Theorem 8, the time derivative of $V(t)$ is given by

$$\begin{aligned} \dot{V}(t) &= \dot{e}_x^T(t)P_x e_x(t) + e_x^T(t)P_x \dot{e}_x(t) + 2Tr[\tilde{\Theta}^T(t)\tilde{\Theta}(t)] \\ &= -e_g^T(t)Q_g e_g(t) + e_x^T(t)Q_x e_x(t) + 2e_x^T(t)P_x \mathbf{b}\tilde{\Theta}(t)x(t) - 2Tr[x(t)e_x^T(t)P_x \mathbf{b}\tilde{\Theta}(t)] \\ &= -e_g^T(t)Q_g e_g(t) - e_x^T(t)Q_x e_x(t). \end{aligned} \quad (3.54)$$

Since $V(t) \geq 0$ and $\dot{V}(t) \leq 0$, it implies that $V(t)$ is a Lyapunov function. Since $V(t) \leq V(0) < \infty$, we have $V(t) \in \mathcal{L}_\infty$ which implies $e_x(t), e_g(t), \tilde{\Theta}(t) \in \mathcal{L}_\infty$. With $h_{cmd}(t) \in \mathcal{L}_\infty$ and (3.41) stable, we have $x_m(t), x_{gm}(t) \in \mathcal{L}_\infty$ which implies that $x(t), x_g(t) \in \mathcal{L}_\infty$. From (3.50) and (3.45) we now have $\dot{e}_x(t), \dot{e}_g(t) \in \mathcal{L}_\infty$.

Furthermore, $\int_0^t \dot{V}(\tau).d\tau = V(t) - V(0)$ and since $V(t)$ is non-increasing and positive definite, we have $V(0) - V(t) \leq V(0)$. Therefore, $-\int_0^t \dot{V}(\tau).d\tau \leq V(0)$ or equivalently $\int_0^t -e_g^T Q_g e_g - e_x^T Q_x e_x.d\tau \leq V(0)$. This implies $e_x(t), e_g(t) \in \mathcal{L}_2$, therefore, from Barbalat's Lemma we have $\lim_{t \rightarrow \infty} e_x(t) = 0$ and $\lim_{t \rightarrow \infty} e_g(t) = 0$. \square

Theorem 9. *Let*

$$\begin{aligned} u(t) &= \Theta_p(t)x_p(t) - Kx(t) \\ &= [[0, \Theta_p(t)] - K]x(t) \end{aligned} \quad (3.55)$$

where $\Theta_p(t)$ is updated as

$$\dot{\Theta}_p(t) = -\mathbf{b}^T P_x e_x(t) x_p^T(t). \quad (3.56)$$

If (i) L_x is chosen such that $[A_m - L_x + \mathbf{b}_m[0, F_p]]$ is Hurwitz and P_x is defined by

$$[A_m - L_x + \mathbf{b}_m[0, F_p]]^T P_x + P_x [A_m - L_x + \mathbf{b}_m[0, F_p]] = -Q_x \quad (3.57)$$

where Q_x is symmetric positive definite and (ii) L_g is chosen such that $[A_g - L_g]$ is Hurwitz, then the system is globally stable and $\lim_{t \rightarrow \infty} e_x(t) = 0$ and $\lim_{t \rightarrow \infty} e_g(t) = 0$.

Proof. With the adaptive control law in (3.55), the error dynamics in (3.44) becomes

$$\begin{aligned} \dot{e}_x(t) &= [A_m - L_x + \mathbf{b}_m[0, F_p]] e_x(t) + \mathbf{b}([0, \Theta_p(t)] - K)x(t) - ([0, \Theta_p^*] - K)x(t) \\ &= [A_m - L_x + \mathbf{b}_m[0, F_p]] e_x(t) + \mathbf{b} \tilde{\Theta}_p(t) x_p(t) \end{aligned} \quad (3.58)$$

where

$$\tilde{\Theta}_p(t) = \Theta_p(t) - \Theta_p^*. \quad (3.59)$$

We define the radially unbounded Lyapunov function candidate

$$V(t) = e_g^T(t) P_g e_g(t) + e_x^T(t) P_x e_x(t) + Tr[\tilde{\Theta}_p^T(t) \tilde{\Theta}_p(t)]. \quad (3.60)$$

Here P_g is the solution to the Lyapunov equation

$$[A_g - L_g]^T P_g + P_g [A_g - L_g] = -Q_g \quad (3.61)$$

where Q_g is symmetric positive definite. It follows that P_x and P_g are positive definite from condition (i) and (ii) of Theorem 8. From (3.45), (3.56), (3.61) and condition (i) of Theorem 9, the time derivative of $V(t)$ is given by

$$\begin{aligned} \dot{V}(t) &= \dot{e}_x^T(t) P_x e_x(t) + e_x^T(t) P_x \dot{e}_x(t) + 2Tr[\tilde{\Theta}_p^T(t) \tilde{\Theta}_p(t)] \\ &= -e_g^T(t) Q_g e_g(t) - e_x^T(t) Q_x e_x(t) + 2e_x^T(t) P_x \mathbf{b} \tilde{\Theta}_p(t) x_p(t) - 2Tr[x_p(t) e_x^T(t) P_x \mathbf{b} \tilde{\Theta}_p(t)] \\ &= -e_g^T(t) Q_g e_g(t) - e_x^T(t) Q_x e_x(t). \end{aligned} \quad (3.62)$$

Since $V(t) \geq 0$ and $\dot{V}(t) \leq 0$, it implies that $V(t)$ is a Lyapunov function. Since $V(t) \leq V(0) < \infty$, we have $V(t) \in \mathcal{L}_\infty$ which implies $e_x(t), e_g(t), \tilde{\Theta}(t) \in \mathcal{L}_\infty$. With $h_{cmd}(t) \in \mathcal{L}_\infty$ and (3.41) stable, we have $x_m(t), x_{gm}(t) \in \mathcal{L}_\infty$ which implies that $x(t), x_g(t) \in \mathcal{L}_\infty$. From (3.50) and (3.45) we now have $\dot{e}_x(t), \dot{e}_g(t) \in \mathcal{L}_\infty$.

Furthermore, $\int_0^t \dot{V}(\tau) d\tau = V(t) - V(0)$ and since $V(t)$ is non-increasing and positive definite, we have $V(0) - V(t) \leq V(0)$. Therefore, $-\int_0^t \dot{V}(\tau) d\tau \leq V(0)$ or equivalently $\int_0^t -e_g^T Q_g e_g - e_x^T Q_x e_x d\tau \leq V(0)$. This implies $e_x(t), e_g(t) \in \mathcal{L}_2$, therefore, from Barbalat's Lemma we have $\lim_{t \rightarrow \infty} e_x(t) = 0$ and $\lim_{t \rightarrow \infty} e_g(t) = 0$. \square

With Theorems 8 and 9, two adaptive controllers have been designed that both insure stability and the control objective in (3.12) are achieved.

Proof of Proposition 7

Through Theorems 8 and 9, we have proved Proposition 7 since the matching condition (3.4) is satisfied and both adaptive controllers in (3.47) and (3.55) take the form of

$$u(t) = \Theta_p(t)x_p(t) + f_p(t) \quad (3.63)$$

as given in (3.5) where $\Theta_p(t), \dot{\Theta}_p(t), f_p(t), \dot{f}_p(t) \in \mathcal{L}_\infty$: Here $f_p(t) = \Theta_{yI}(t)e_{yI}(t)$ in (3.47) of Theorem 8 and $f_p(t) = Kx(t)$ in (3.55) of Theorem 9. Therefore, we may use the sticking analysis as presented in Table 3.1. Simulations are included in the following section in order to demonstrate the impact of inner-loop sticking on outer-loop control.

3.3.4 Simulation Study with Sticking Analysis

We carry out a simulation study in this section to demonstrate the impact sticking as presented in Section 3.2. Two adaptive controllers are simulated: The first corresponds to Theorem 8 (*Controller 1*) and the second corresponds to Theorem 9 (*Controller 2*).

Defining the Adaptive System and Control Objective

The plant model is given by (3.38) and (3.18) with the stability and control derivatives from Section 3.3.1. For both controllers, the CRM is chosen as in (3.41). The parameters of the CRM are as previously specified in Section 3.3.2 and the error state feedback matrices are chosen with

$$L_x = \begin{bmatrix} 5 & 0 \\ 0 & 5 \end{bmatrix} \quad L_g = \begin{bmatrix} 1 & 0 \\ 0 & 1 \end{bmatrix}. \quad (3.64)$$

With these parameters and feedbacks, all the necessary stability criterion from Theorems 8 and 9 are satisfied. *Controller 1* follows the design in (3.47) through (3.49) from Theorem 8. *Controller 2* follows the design in (3.55) through (3.57) from Theorem 9.

The Lyapunov equation in (3.49) for *Controller 1* was solved with solved with $Q_x = I$. *Controller 2* uses the same Lyapunov equation solution in (3.57). We specify the altitude command signal in (3.12) with

$$h_{cmd}(t) = \begin{cases} 0 & 0 \leq t < 50 \\ 100 & t \geq 50 \end{cases}. \quad (3.65)$$

The control objective is to track the command signal $h_{cmd}(t)$ as given in (3.12).

Application of the Sticking Analysis

For both *Controller 1* and *Controller 2*, we have proven Proposition 7, thus we may use the sticking analysis as presented in Table 3.1. In order to investigate the impact of this inner-loop sticking on outer-loop control, we must define $G(s)$ as given in (3.11). Let us define

$$\begin{bmatrix} \dot{x}_{ORM} \\ \dot{x}_{gORM} \end{bmatrix} = \begin{bmatrix} A_m + [0_{(n_p+1) \times 1}, \mathbf{b}_m F_p] & \mathbf{b}_m F_g \\ [0_{n_g \times 1}, B_g] & A_g \end{bmatrix} \begin{bmatrix} x_{ORM} \\ x_{gORM} \end{bmatrix} + \begin{bmatrix} \mathbf{b}_m F_{cmd} \\ 0_{n_g \times 1} \end{bmatrix} h_{cmd}(t) \quad (3.66)$$

which represents the ORM from (3.35) and therefore the desired output of the plant. From (3.41), (3.45) and (3.66) we obtain

$$\begin{bmatrix} \dot{x}_m - \dot{x}_{ORM} \\ \dot{x}_{gm} - \dot{x}_{gORM} \\ \dot{e}_g \end{bmatrix} = \begin{bmatrix} A_m + [0_{(n_p+1) \times 1}, \mathbf{b}_m F_p] & \mathbf{b}_m F_g \\ [0_{n_g \times 1}, B_g] & A_g \\ 0_{n_g \times (n_p+1+n_g)} & A_g - L_g \end{bmatrix} \begin{bmatrix} \mathbf{b}_m F_g \\ L_g \\ e_g \end{bmatrix} + \begin{bmatrix} L_x \\ [0_{n_g \times 1}, B_g] \\ 0_{n_g \times (n_p+1)} \end{bmatrix} e_x(t). \quad (3.67)$$

From (3.40), we note that $x_g(t) - x_{gORM}(t) = x_{gm}(t) - x_{gORM}(t) + e_g(t)$, thus the transfer function $G(s)$

$$x_g(s) - x_{gORM}(s) = G(s)e_x(s) \quad (3.68)$$

may be obtained from (3.67). Let

$$e_x(t) = \begin{bmatrix} e_{yI}(t) \\ \alpha(t) \\ q(t) \end{bmatrix} - \begin{bmatrix} e_{yIm}(t) \\ \alpha_m(t) \\ q_m(t) \end{bmatrix} = \begin{bmatrix} e_{yI}(t) - e_{yIm}(t) \\ e_{x\alpha}(t) \\ e_{xq}(t) \end{bmatrix} \quad (3.69)$$

and

$$x_g(t) - x_{gORM}(t) = \begin{bmatrix} \theta(t) \\ h(t) \end{bmatrix} - x_{gORM}(t) = \begin{bmatrix} x_g \theta(t) - x_{gORM} \theta(t) \\ x_g h(t) - x_{gORM} h(t) \end{bmatrix}. \quad (3.70)$$

The Bode plots of $e_x(s)$ to $x_g(s) - x_{gORM}(s)$ are shown in Figure 3-7. We know that $x_{gORM}(t)$ represents the desired outer-loop output of the plant. If inner-loop sticking imposes the constraint $\tilde{x}_p(t) \in \mathbf{N} \forall t \in [t_1, t_2]$ such that $\|e_x(t)\| > 0 \forall t \in T$, then $x_g(t)$ will converge slowly to the desired output represented by the ORM. This is true since $x_g(t) - x_{gORM}(t)$ is sensitive to $e_x(t)$ as shown in Figure 3-5. Simulation results are included in the following section to demonstrate this impact of sticking.

Simulation Results

With the adaptive control systems defined, we can now complete the simulations. We choose the initial conditions at $t_1 = 0$ with

$$x(t_1) = x_m(t_1) = 0 \quad x_g(t_1) = x_{gm}(t_1) = 0. \quad (3.71)$$

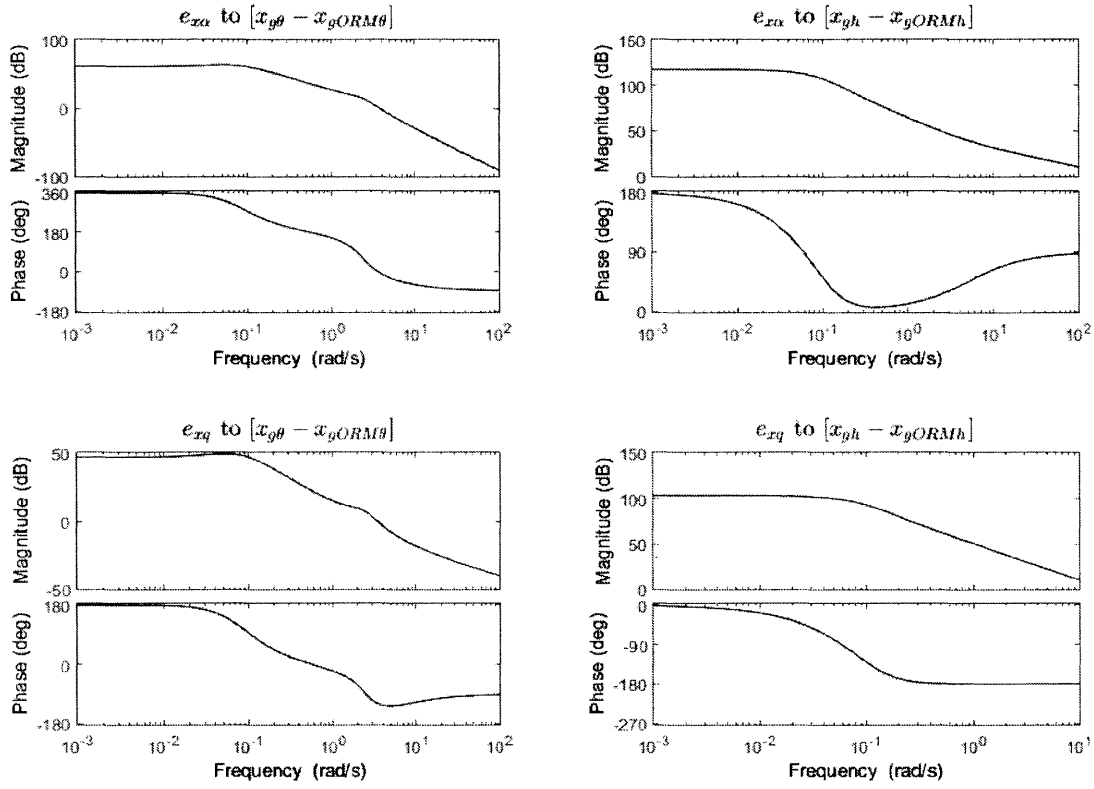


Figure 3-7: Bode plots for the transfer functions from $e_x(s)$ to $x_p(s) - x_{SORM}(s)$

For both adaptive controllers in (3.47) and (3.55), we initialize the parameter $\Theta_p(t)$ at $t_1 = 0$ with

$$\tilde{\Theta}_p(t_1) = k \|\Theta_p^*\| [1, 1] \quad (3.72)$$

where $\tilde{\Theta}_p(t) = \Theta_p(t) - \Theta_p^*$ and k is an arbitrary constant. For *Controller 1* we also initialize the parameter $\Theta_{yI}(t)$ at $t_1 = 0$ which minimizes $\tilde{\Theta}(t_1)$ defined in (3.51), thus the parameters of both controllers are initialized with equivalent uncertainty.

At this point, each adaptive control system is fully defined and all the initial conditions are given. We now consider the sticking analysis as presented in Section 3.2. It should be noted that the variables Θ_{p0} , \hat{A}_{p0} , α , γ , β , $\delta\theta_p^*$, f^* and f_d^* as well as the sets \mathbf{S} and \mathbf{N} to be used in the remainder of this section, are as defined in Table 3.1. Additionally, Theorems 2 and 6 also refer to that provided in Table 3.1.

If $\Theta_{p0} = \tilde{\Theta}_p(t_1)$, then the initialization in (3.72) establishes a Hurwitz \hat{A}_{p0} for $k \geq 1$ such that a sticking region may be defined for both *Controller 1* and *Controller 2* following

Theorem 6. The first set of simulations are completed for $k = 1$ when the effects due to sticking are negligible. The altitude response $h(t)$, command signal $h_{cmd}(t)$ and elevator input $u(t)$ are shown against time in Figure 3-8. It is clear that there is no significant difference between *Controller 1* and *Controller 2* when the effects of sticking are negligible.

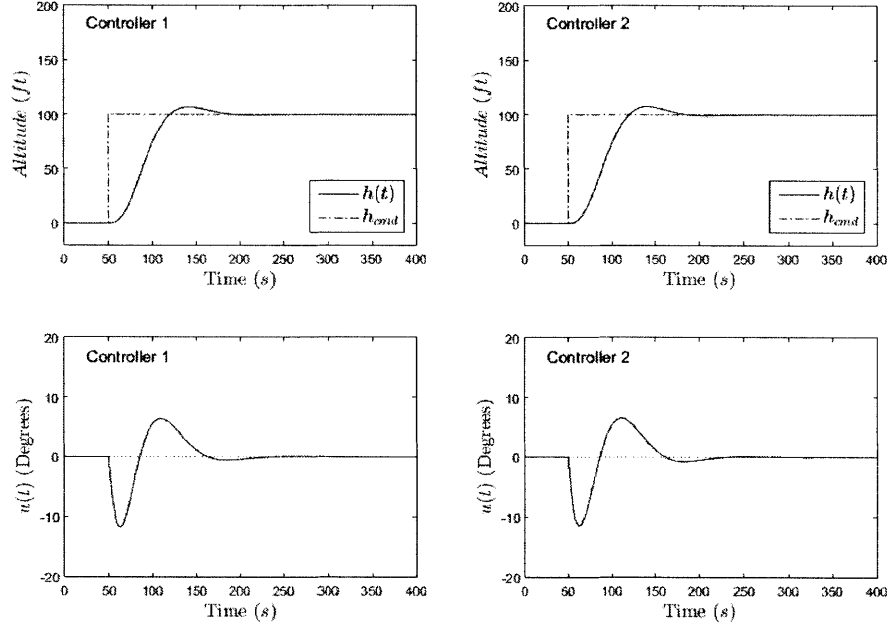


Figure 3-8: Altitude response $h(t)$, command signal $h_{cmd}(t)$ and elevator input $u(t)$ versus time for $k = 1$

Consider now the same set of results shown in Figure 3-9 when $k = 10$: This time we notice a large difference between the response of *Controller 1* and *Controller 2*. To explain why *Controller 2* does not converge quickly to the desired output, we complete a sticking analysis for the case when $k = 10$. Let

$$\Theta_{p0} = \tilde{\Theta}_p(t_1) = 10 \|\Theta_p^*\| [1, 1] = [32.49, 32.49] \quad (3.73)$$

and $\gamma = 1$, then \hat{A}_{p0} is Hurwitz and S is defined in Theorem 6 with $\delta\theta_p^* = 2.50$ as

$$S : \left\{ \tilde{\Theta}_p \in \mathbb{R}^2 \mid - \begin{bmatrix} 2.50 \\ 2.50 \end{bmatrix}^T \leq \tilde{\Theta}_p + \begin{bmatrix} 32.49 \\ 32.49 \end{bmatrix}^T \leq \begin{bmatrix} 2.50 \\ 2.50 \end{bmatrix}^T \right\}.$$

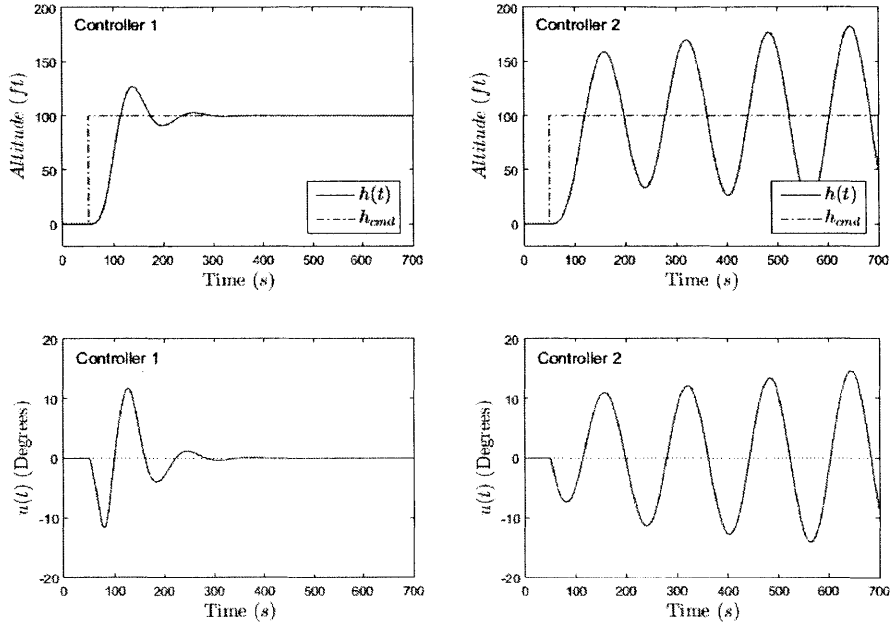


Figure 3-9: Altitude response $h(t)$, command signal $h_{cmd}(t)$ and elevator input $u(t)$ versus time for $k = 10$

From the simulation we may define f^* and f_d^* for each controller and select β as small as possible with $\alpha = 0.5$. This is given by

$$\text{Controller 1 : } f_p(t) = \Theta_{yI}(t)e_{yI}(t) \rightarrow f^* = 3.87 \quad f_d^* = 0.248 \rightarrow \beta = 0.0338$$

$$\text{Controller 2 : } f_p(t) = Kx(t) \rightarrow f^* = 4.57 \quad f_d^* = 0.181 \rightarrow \beta = 0.0339.$$

We then have set \mathbf{N} defined for each controller with

$$\text{Controller 1 : } \mathbf{N} : \left\{ \tilde{x} \in \mathbb{R}^2 \mid \tilde{x}^T \begin{bmatrix} 2.026 & 0.022 \\ 0.022 & 0.026 \end{bmatrix} \tilde{x} \leq 0.0092 \right\}$$

$$\text{Controller 2 : } \mathbf{N} : \left\{ \tilde{x} \in \mathbb{R}^2 \mid \tilde{x}^T \begin{bmatrix} 2.026 & 0.022 \\ 0.022 & 0.026 \end{bmatrix} \tilde{x} \leq 0.0093 \right\}.$$

Figure 3-10 includes the time response of the parameters $[\Theta_{yI}(t), \Theta_p(t)]$ for *Controller 1* and $\Theta_p(t)$ for *Controller 2*. This figure also illustrates how the error parameters $\tilde{\Theta}_p(t)$ traverse through \mathbf{S} , where it can be seen that $\tilde{\Theta}_p(t) \in \mathbf{S} \forall t \in [0, 700]$ for both controllers. Therefore, since $\tilde{x}_p(t_1) = x_p(t_1) = 0$, the conditions of Theorem 2 are satisfied. It follows

that $\tilde{x}_p(t) \in \mathbf{N} \forall t \in [0, 700]$ for both systems as also shown in Figure 3-10.

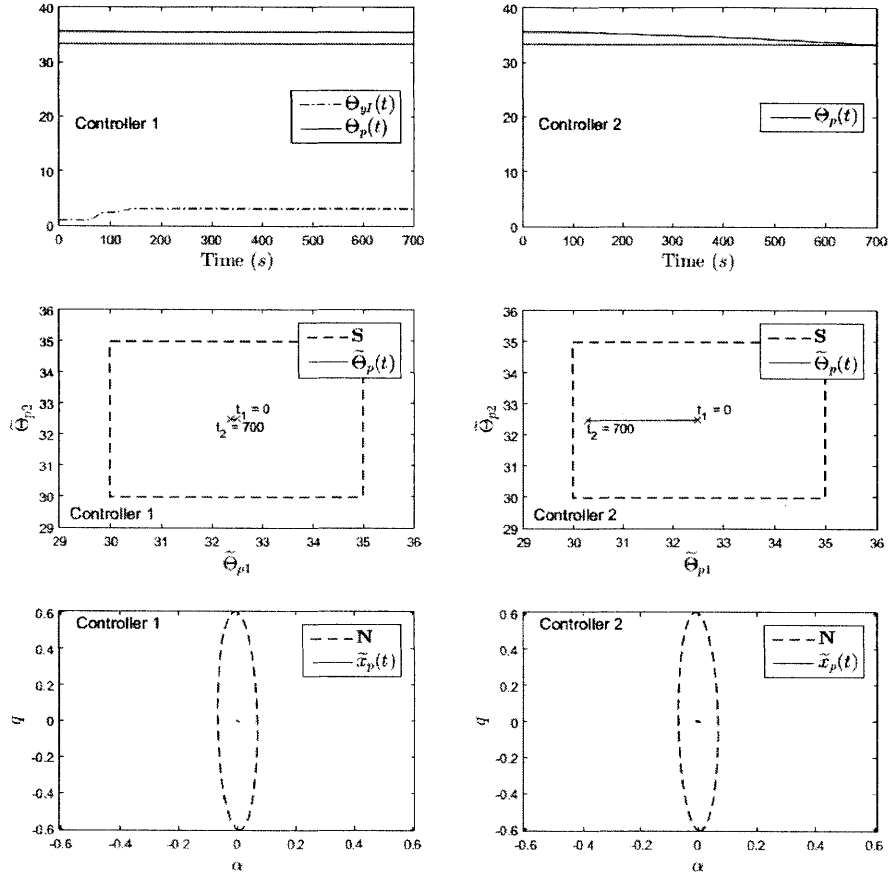


Figure 3-10: Inner-loop sticking in *Controller 1* and *Controller 2* for $t \in [0, 700]$ with $k = 10$

To explain why *Controller 2* does not converge quickly to the desired output, consider the trajectory of $\tilde{x}_{pm}(t) = x_{pm}(t) - \hat{x}_p(t)$ superimposed over \mathbf{N} on the time interval $t \in [0, 700]$ as shown in Figure 3-11, where $\tilde{x}_p(t) = [\tilde{\alpha}(t), \tilde{q}(t)]$ and $\tilde{x}_{pm}(t) = [\tilde{\alpha}_m(t), \tilde{q}_m(t)]$. Here we see that $x_p(t)$ is unable to track $x_{pm}(t)$ for *Controller 2* due to the imposed constraint $\tilde{x}_p(t) \in \mathbf{N} \forall t \in [0, 700]$ caused by the inner-loop sticking. This is in contrast *Controller 1* where $x_p(t)$ is able to effectively track $x_{pm}(t)$ inside \mathbf{N} . For *Controller 2* this implies that $\exists T \subset [0, 700]$ such that $\|e_x(t)\| > 0 \forall t \in T$. From the discussion in Section 3.2.2 and the Bode plots of $G(s)$ in Figure 3-7, we see that the inner-loop sticking will cause slow convergence in the outer-loop for *Controller 2*. Only once *Controller 2* eventually leaves the sticking region, can the desired output be achieved as shown in Figure 3-12.

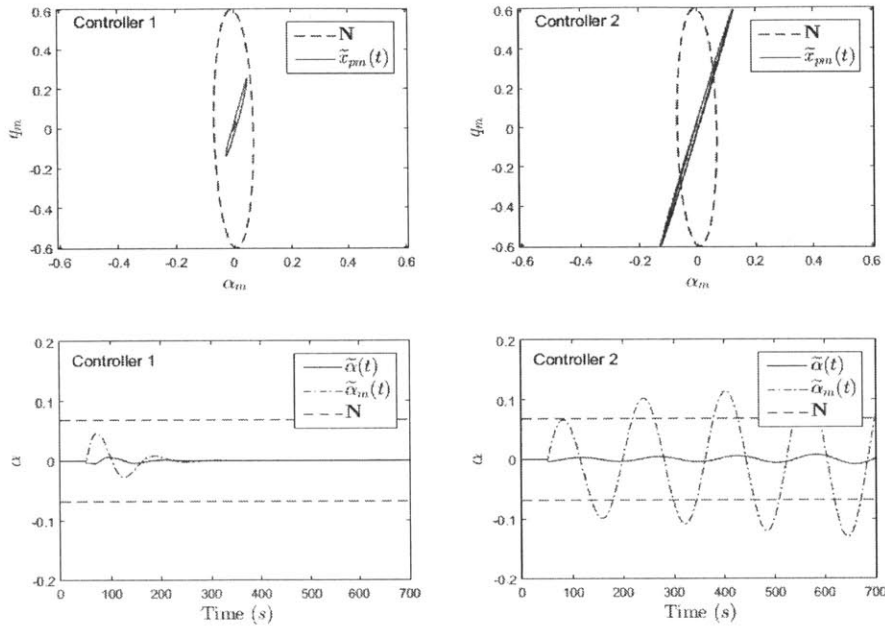


Figure 3-11: $\tilde{x}_{pm}(t)$ superimposed over \mathbf{N} for *Controller 1* and *Controller 2* for $t \in [0, 700]$ with $k = 10$

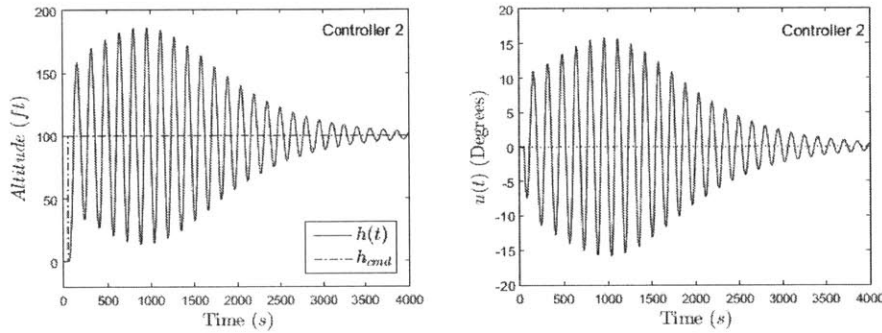


Figure 3-12: Altitude response $h(t)$, command signal $h_{cmd}(t)$ and elevator input $u(t)$ of *Controller 2* versus time for $k = 10$ and $t \in [0, 4000]$

3.4 Summary

In this chapter, we have focused on the impact of inner-loop sticking on outer-loop control. Following Chapter 2, an analysis is presented that identifies the existence a sticking region in the inner-loop and its impact on command following in the outer-loop. A practical

application of adaptive control is presented with a combined inner and outer-loop problem for an aircraft autopilot system. Simulations are included for the autopilot system with a sticking analysis to demonstrate the impact of inner-loop sticking on outer-loop control.

Chapter 4

Concluding Remarks

In Chapter 2, the convergence properties of errors are examined in a class of adaptive systems that corresponds to adaptive control of linear time-invariant plants with state variables accessible. The existence of a sticking region is demonstrated in the error space where the state errors move with a finite velocity independent of their magnitude. These properties are exhibited by ORM, CRM and IC-adaptive systems.

Through simulation and numerical studies, it is shown that a system may traverse through the sticking region for an extended period of time, which reduces the rate at which the system reaches the control objective. Although a sticking region is defined for the ORM, CRM and IC-adaptive systems, it is shown that each system is effected differently by sticking. The analysis in Chapter 2 allows us to investigate the susceptibility of each system to sticking effects. It is shown that the IC-adaptive system demonstrates a faster transient performance during sticking compared to the ORM and CRM-adaptive systems with A unknown. When additional uncertainty is present in the ORM and CRM-adaptive systems such that $(A, \lambda \mathbf{b})$ is unknown, then an improved transient performance during sticking is demonstrated.

In Chapter 3, the impact of sticking is investigated for outer-loop controllers that implement inner-loop adaptation. An analysis is presented that identifies the existence a sticking region in the inner-loop and its impact on command following in the outer-loop. To demonstrate these sticking effects in outer-loop control, we focus on a combined inner and outer-loop problem in a flight control application. Two adaptive controllers are designed,

for which stability was proved similarly. However, despite the similarities, the controllers exhibit different transient behaviors during sticking which has major implications on outer-loop tracking.

In this thesis, it is shown that the convergence properties of errors in adaptive systems may be characterized by the existence of sticking regions. It is demonstrated that these sticking regions may greatly impact the transient performance of an adaptive system. We therefore learn that it is important to consider the susceptibility of an adaptive system to sticking.

Bibliography

- [1] O. Amidi, and C. Thorpe, "Integrated Mobile Robot Control," Proceedings of SPIE: The International Society for Optical Engineering, vol. 1388, pp 505-523, 1991.
- [2] H.E. Bell, "Gerschgorin's Theorem and the Zeros of Polynomials," The American Mathematical Monthly, vol. 72, no. 3, pp. 292-295, 1965.
- [3] J. Deyst, and J.P. How, "Performance and Lyapunov Stability of a Nonlinear Path-Following Guidance Method," Journal of Guidance, Control and Dynamics, vol. 30, no. 6, pp 1718-1728, 2007.
- [4] F. Gavilan, R. Vazquez, and E.F. Camacho, "An Iterative Model Predictive Control Algorithm for UAV Guidance," IEEE Transactions on Aerospace and Electric Systems, vol. 51, no. 3, July 2015.
- [5] T.E. Gibson, A.M. Annaswamy, and E. Lavretsky, "On adaptive control with closed-loop reference models: Transients, oscillations, and peaking," IEEE Access, vol. 1, pp. 703-717, 2013.
- [6] T.E. Gibson, A.M. Annaswamy, and E. Lavretsky, "Closed-Loop Reference Models in Adaptive Control, Part 1: Transient Performance," American Control Conference, IEEE, Washington DC, pp. 3376-3383, 2013.
- [7] W.P.M.H. Heemels, and M.K. Camlibel, "Controllability of Linear Systems with Input and State Constraints," Proceedings of the 46th IEEE Conference on Decision and Control, New Orleans, LA, 2007.
- [8] B.M. Jenkins, T.E. Gibson, A.M. Annaswamy, and E. Lavretsky, "Asymptotic stability and convergence rates in adaptive systems," IFAC Workshop on Adaptation and Learning in Control and Signal Processing, Caen, France, 2013.
- [9] E. Lavretsky, and K.A. Wise, "Robust and Adaptive Control With Aerospace Applications," London: Springer-Verlag, 2013, ch. 1, 10.
- [10] K.S. Narendra, and A.M. Annaswamy, "Stable Adaptive Systems," New York: Dover, 2005.
- [11] A. Ollero, and G. Heredia, "Stability Analysis of Mobile Robot Path Tracking," Proceedings of the Institute of Electrical and Electronics Engineers, IEEE, Piscataway, NJ, pp. 461-466.

- [12] S. Park, J. Deyst, and J.P. How, "A New Guidance Logic for Trajectory Tracking," AIAA Guidance, Navigation, and Control Conference and Exhibit, August 2004.
- [13] V. Stepanyan, and K. Krishnakumar, "MRAC Revisited: Guaranteed Performance with Reference Model Modification," American Control Conference, 2010.
- [14] D.P. Wiese, A.H. Annaswamy, and E. Lavretsky, "Sequential Loop Closure Based Adaptive Autopilot Design for a Hypersonic Vehicle," pp. 1-19